Elastic and magnetoelastic relaxation behaviour of multiferroic (ferromagnetic + ferroelectric + ferroelastic) $Pb(Fe_{0.5}Nb_{0.5})O_3$ perovskite

2015 J. Phys.: Condens. Matter 27 285901

(http://iopscience.iop.org/0953-8984/27/28/285901)

OPEN ACCESS
IOP Publishing
Journal of Physics: Condensed Matter
J. Phys.: Condens. Matter **27** (2015) 285901 (18pp)
doi:10.1088/0953-8984/27/28/285901

Elastic and magnetoelastic relaxation behaviour of multiferroic (ferromagnetic + ferroelectric + ferroelastic) $Pb(Fe_{0.5}Nb_{0.5})O_3$ perovskite

M A Carpenter[1], J A Schiemer[1], I Lascu[1], R J Harrison[1], A Kumar[2], R S Katiyar[3], N Ortega[3], D A Sanchez[3], C Salazar Mejia[4], W Schnelle[4], M Echizen[5], H Shinohara[5], A J F Heap[5], R Nagaratnam[5], S E Dutton[5] and J F Scott[5]

[1] Department of Earth Sciences, University of Cambridge, Downing Street, Cambridge CB2 3EQ, UK
[2] National Physical Laboratory (CSIR), New Delhi 110012, India
[3] Institute for Functional Nanomaterials, University of Puerto Rico, PO Box 23334, San Juan, 00931-3334, Puerto Rico
[4] Max Planck Institute for Chemical Physics of Solids, Nöthnitzer Strasse 40, 01187 Dresden, Germany
[5] Cavendish Laboratory, University of Cambridge, Madingley Road, Cambridge CB3 0HE, UK

E-mail: mc43@esc.cam.ac.uk

Received 8 March 2015, revised 6 May 2015
Accepted for publication 12 May 2015
Published 30 June 2015

Abstract

Resonant Ultrasound Spectroscopy has been used to characterize elastic and anelastic anomalies in a polycrystalline sample of multiferroic $Pb(Fe_{0.5}Nb_{0.5})O_3$ (PFN). Elastic softening begins at ~550 K, which is close to the Burns temperature marking the development of dynamical polar nanoregions. A small increase in acoustic loss at ~425 K coincides with the value of T^* reported for polar nanoregions starting to acquire a static or quasi-static component. Softening of the shear modulus by ~30–35% through ~395–320 K, together with a peak in acoustic loss, is due to classical strain/order parameter coupling through the cubic → tetragonal → monoclinic transition sequence of ferroelectric/ferroelastic transitions. A plateau of high acoustic loss below ~320 K is due to the mobility under stress of a ferroelastic microstructure but, instead of the typical effects of freezing of twin wall motion at some low temperature, there is a steady decrease in loss and increase in elastic stiffness below ~85 K. This is attributed to freezing of a succession of strain-coupled defects with a range of relaxation times and is consistent with a report in the literature that PFN develops a tweed microstructure over a wide temperature interval. No overt anomaly was observed near the expected Néel point, ~145 K, consistent with weak/absent spin/lattice coupling but heat capacity measurements showed that the antiferromagnetic transition is actually smeared out or suppressed. Instead, the sample is weakly ferromagnetic up to ~560 K, though it has not been possible to exclude definitively the possibility that this could be due to some magnetic impurity. Overall, evidence from the RUS data is of a permeating influence of static and dynamic strain relaxation effects which are attributed to local strain heterogeneity on a mesoscopic length scale. These, in turn, must have a role in determining the magnetic properties and multiferroic character of PFN.

Keywords: multiferroic, perovskite, elastic relaxations

(Some figures may appear in colour only in the online journal)

1. Introduction

Phases with the perovskite structure in the solid solutions $Pb(Zr_{0.53}Ti_{0.47})O_3$ (PZT)–$Pb(Fe_{0.5}Nb_{0.5})O_3$ (PFN) and $Pb(Zr_{0.53}Ti_{0.47})O_3$–$Pb(Fe_{0.5}Ta_{0.5})O_3$ (PFT) have recently been shown to display simultaneous ferromagnetic and ferroelectric properties at room temperature [1–4]. Control of ferroelectric domain patterns by application of a magnetic field has also been demonstrated [5]. These materials are the lowest-loss room-temperature multiferroics currently known [1]. They combine aspects of the properties of the pure, end member phases to produce ferromagnetism, antiferromagnetism, ferroelectricity and ferroelasticity. In general, the main focus of attention when dealing with multiferroic materials is on the magnetic and dielectric properties. Somewhat less attention tends to be paid to the role of strain even though it is widely recognized to provide an important indirect mechanism for magnetoelectric coupling and is likely be an important factor in pinning and switching behaviour. As part of a wider study of the elastic and anelastic properties of selected phases from the PFN–PZT and PFN–PZT solid solutions, aspects of the ferroelastic behaviour of a ceramic sample of end-member PFN which displays ferromagnetism at room temperature have been investigated by resonant ultrasound spectroscopy (RUS). Here we present results which draw attention to the permeating presence of static and dynamic strain coupling effects.

The structure and properties of PFN have been studied in great detail since the original report of ferroelectric and antiferromagnetic transitions by Bokov *et al* [6]. To summarize many of the references discussed below, the current general view for ceramic and single crystal samples which are single phase, stoichiometric and homogeneous, is that they are ferroelectric below $T_c \approx 385$ K (reported values in the range ~370–400 K) and G-type antiferromagnetic below $T_N \approx 150$ K (reported values in the range ~143–160 K). Weak ferromagnetism due to the development of a spin-glass then coexists with the antiferromagnetic ordering below ~10–30 K. In more detail, the transition at T_c is from a parent cubic structure with space group $Pm\bar{3}m$ (or $Fm\bar{3}m$ for a structure with B-site cation order) to a tetragonal structure with space group $P4mm$. Lattice parameter variations [7, 8], changes in the remanent electric polarization [9] and birefringence data [10] appear to show the transition as being thermodynamically continuous. However, a hysteresis of ~4 K [11] and 17 K [12] has also been reported for the transition point between heating and cooling, suggesting first order character. A heat capacity anomaly with its peak at 374 ± 1 K [13] has the form qualitatively similar to that expected for Landau tricritical and, hence, is at least consistent with the ferroelectric/ferroelastic transition being close to the boundary between second order and first order. A second transition with first order character occurs ~20–40 K below T_c, to another ferroelectric structure which was first treated as being rhombohedral ($R3m$) but is now thought to be monoclinic (Cm) [7, 8, 10, 14–22]. Some samples may really be rhombohedral, however (e.g. [23]). Softening of a zone centre transverse optic mode with increasing temperature between 3 and ~350 K has been observed by inelastic neutron scattering, consistent with a soft mode mechanism driving the ferroelectric transitions [24].

The antiferromagnetic ordering transition has been followed via the continuous reduction in intensity of the (1/2,1/2,1/2) reflection in neutron diffraction patterns [25–27], but the Néel point is identified in most studies by a small anomaly in the magnetic susceptibility. Magnetoelectric coupling was recognized by Astrov *et al* [28] and is indicated by variations in electric polarization as a function of magnetic field at 15 K [25] and below 10 K [29], small changes in dielectric properties under the influence of an external magnetic field at room temperature [30] and as a function of temperature [31], changes in dielectric properties in the vicinity of the Néel point [32–37] and as changes in magnetic susceptibility near T_c [9, 38, 39]. Finally, spin glass like behaviour has been proposed to occur below ~120 K [40], ~80 K [24] or ~50 K [26, 41], while reported values of the glass transition temperature, T_g, are in the range 10–30 K [26, 40–44].

If PFN and its derivatives obtained by chemical substitution showed only the three transitions referred to above, they would probably not attract quite so much attention in the context of 'useful' magnetoelectric properties. However, even PFN itself shows great variability between samples and, in particular, it can be weakly ferromagnetic at room temperature in both bulk samples [39, 45, 46] and thin films [36, 47–50]. The upper temperature limit reported for ferromagnetic properties includes 530–580 K [46], 370 K [39], 150 K [51], T_N [33, 52–54] and 137 K [35]. The ferroelectric transition shows some aspects of relaxor behaviour in having a broad peak in the real part of the dielectric permittivity, ε', through T_c, (e.g. [34, 37, 50, 55–64]. Although this peak in ε' occurs at a temperature which is typically independent of measuring frequency, some samples show a frequency dependence [65–67] and a Vogel–Fulcher freezing temperature of 280 K has reported in one case [67]. The diffuseness of the transition is generally ascribed to the effects of local variations in composition associated with Fe/Nb order/disorder.

No diffraction evidence has yet been found for long range order of Fe^{3+} and Nb^{5+} on crystallographic B-sites (e.g. [15, 17, 21, 23, 32, 61, 68]), but Mössbauer [69, 70] and NMR [71] spectroscopy provide evidence of chemically/crystallographically distinct B-sites, implying that there is some degree of short range Fe/Nb ordering or clustering. The presence of Raman bands which would be forbidden in spectra from a crystal with space group $Pm\bar{3}m$ has also been used to demonstrate that the local symmetry of both thin film and bulk PFN

must be lowered [72, 73]. Although the radii of Fe^{3+} and Nb^{5+} are quite similar, their charge difference might be sufficient to drive the ordering and Correa *et al* [73] have argued that the local symmetry is actually $Fm\bar{3}m$ with a $2 \times 2 \times 2$ lattice (alternating Fe/Nb/Fe/Nb…. in 3D). Variations in the degree of this order and/or the size of ordered clusters, depending on the sample preparation and thermal history, would be expected to give rise to variations in the relaxor character of the ferroelectric transitions. The B-site order/disorder could also contribute to variations in the magnetic ordering either directly, or indirectly through magnetoelectric coupling to ferroelectric displacements, with implications for the character of the antiferromagnetic transition. In contrast with the intensity of the (1/2,1/2,1/2) reflection in neutron diffraction patterns indicative of long range ordering going smoothly to zero at T_N [25, 26], diffraction data from the single crystal sample of Stock *et al* [24] do not show a discrete phase transition. There is a steep decrease in intensity with increasing temperature through 150 K but some intensity remains at least up to ~400 K. Likewise, heat capacity data of Yang *et al* [54] do not show any anomaly near 150 K that would indicate the existence of a discrete antiferromagnetic ordering transition.

Evidence for a temperature, T_d, below which dynamic polar nanoregions (PNRs) develop in bulk samples (commonly referred to as the Burns temperature) is provided both by acoustic emission data (564–603 K [12]) and a subtle change in thermal expansion (~690 K [74]). A similar change in thermal expansion has also been used to indicate $T_d \approx 640$ K in a thin film deposited on $SrTiO_3$ [49]. T^*, the temperature below which PNRs start to acquire some static component, has been most recently placed at ~430 K for a bulk sample [12] and ~510 K for a thin film [49]. The second transition, ~20–40 K below T_c, generally seems to have no influence on the temperature dependence of the dielectric permittivity [32, 34, 37, 45, 50, 55, 57, 58, 63, 64, 67, 75], but is sometimes seen as an shoulder on the main peak [65, 76]. Mabud [16] only found evidence for a single transition in powder x-ray diffraction patterns collected between room temperature and 423 K.

If there are variations in electric polarization in PFN, either locally in the form of PNRs or as long range correlations below T_c, and there is also magnetoelectric coupling, it follows that there must be local and longer range variations in magnetic order. This has to be a significant factor in the differences in magnetic properties between samples which are only ferromagnetic below T_g and those which also have a weak ferromagnetic moment over wide temperature intervals. Diffuse scattering around the magnetic reflections in single crystal neutron diffraction patterns at $T > T_N$ [25, 26] show that local ordering occurs above the Néel point and evidence from electron paramagnetic resonance spectra is for the development of local clusters of antiferromagnetic order in a temperature interval of perhaps up to ~40 K above T_N [35, 41, 53, 71]. The absence of an overt anomaly in the heat capacity [54] is perhaps further evidence that the total entropy change associated with the development of long range order below T_N can be spread over a relatively wide temperature interval, at least in some samples.

A model which is commonly referred to in the literature is based on that of Rotaru *et al* [43] and Kleemann *et al* [44], in which there is a coexistence of percolating antiferromagnetic clusters which have long range order below T_N, and superantiferromagnetic clusters which have uncompensated magnetic moments. The spin glass behaviour below ~20 K is then due to freezing of correlations between the uncompensated moments to give a weak ferromagnetic moment. Alternatively, the antiferromagnetic ordering is more homogeneous but the individual spins have a degree of canting with tilt angles that are random from site to site [21, 26]. In this case the spin glass transition would be due to freezing of correlations of the tilt angles [26]. Spin canting has also been proposed to explain the ferromagnetism detected in some samples at higher temperatures [45]. Under monoclinic symmetry all that would be needed to induce preferred alignments of the canting moments would be a field arising from some other aspect of the crystal structure, but this mechanism would presumably only apply if there was already long range or local antiferromagnetic order. The origin of weak ferromagnetic ordering above T_N has not been fully explained but could be due to coupling between 'local polarization and magnetization in superparamagnetic polar nanoclusters' [39], or to superantiferromagnetic clusters which develop weak excess moments [49]. The most recent calculations also focus on the role of clustering derived from short range B-site chemical ordering [77, 78].

From this brief review of the remarkably variable properties of PFN, it is apparent that an important common thread is inhomogeneity at a local length scale. It is likely that there is chemical inhomogeneity due to local order and disorder of Nb and Fe on crystallographic B sites, inhomogeneity of ferroelectric polarization from PNRs and ferroelectric domain walls, plus inhomogeneity due to magnetic fluctuations, superparamagnetic clusters, superantiferromagnetic clusters and spin canting. It follows that if samples prepared by different routes have different degrees of short range order or PNR configurations they will have differences in their magnetic properties. The magnetoelectric coupling mechanism is believed to occur at least in part by strain mediation (e.g. [34, 37, 39, 49, 63]), and if there is any coupling of strain with the atomic ordering, magnetic ordering or ferroelectric displacements it is inevitable that local variations of these will be accompanied by local variations in strain. Direct evidence of strain heterogeneity on a scale of ~10–30 nm is provided by tweed microstructures existing from ~385 K down to at least ~110 K, observed by transmission electron microscopy in a single crystal grown by a modified Bridgman method [79].

Any strain relaxation accompanying the ferroelectric and magnetic transitions is likely to be seen in variations of elastic and anelastic properties. Three different sets of data reported in the literature already show significant softening of bulk elastic constants (~10 MHz [37, 58, 80], ~800 Hz [81], or unspecified frequencies [56, 82]) and peaks of acoustic loss [58, 81, 82] with falling temperature from above the ferroelectric transition. There are smaller anomalies in elastic and anelastic properties through T_N [37, 63, 80, 81], but additional effects have been also reported at ~110 K and ~250 K [37, 58, 80]. The acoustic loss measured at 10 MHz appears to consist

of a series of overlapping peaks and remains high between T_c and T_N [37, 58]. In the present study elastic and anelastic properties have been followed through T_g, T_N, T_c, T^* and T_d by RUS in the frequency range ~0.1–1 MHz, with the specific aim of determining the character and dynamics of strain relaxation behaviour in an important end-member perovskite phase which contains local chemical and structural heterogeneity.

2. Sample description and experimental methods

The ceramic sample of $PbFe_{0.5}Nb_{0.5}O_3$ was prepared by a conventional solid state reaction route following a methodology closely similar to that described by Sanchez *et al* [1]. Starting materials were analytical purity oxides, PbO, Fe_2O_3 and Nb_2O_5, which were ball milled together in methanol 25 times for 40 min at 600 rpm. After evaporation of the methanol at 50 °C, the dried mixture was reground and passed through a 250 μm sieve. The resulting powder was placed in a closed crucible, heated to 400 °C at 10 °C min^{-1} and held there for 3 h. It was then heated to 850 °C at the same rate and held at this temperature for a further 10 h, followed by cooling to room temperature at 10 °C min^{-1}. After further grinding and passing through a 180 μm sieve, the formation of perovskite was confirmed by x-ray diffraction. Finally, a pellet was prepared with poly vinyl alcohol as a binder. This was heated to 600 C at 10 °C min^{-1} and held for 3 h to evaporate the binder. The final stage was heating to 1050 °C at the same rate, annealing at this temperature for 4 h and cooling back to room temperature, again at 10 °C min^{-1}. In order to prevent PbO loss during the high temperature sintering, and thereby maintain the desired stoichiometry, an equilibrium PbO vapour was established with $PbZrO_3$ as setter in the covered alumina crucible. The form of the final sample was a flat, hard disc with diameter ~9 mm and thickness ~0.65 mm. This was cut into smaller pieces for the different measurements described below.

A powder x-ray diffraction pattern was obtained at room temperature with a PANalytical Empyrean x-ray diffractometer (CuKα, $\lambda = 1.5406$ Å) from one ground up portion of the pellet. Data were collected over the angular range $10 \leqslant 2\theta \leqslant 90°$ with steps of $\Delta 2\theta = 0.04°$. The x-ray pattern could be modelled using a cubic perovskite structure, and Rietveld refinement [83] using the FULLPROF suite of programs [84] gave a lattice parameter of $a = 4.0134(1)$ Å. An additional weak peak at $2\theta \approx 29.2°$ with intensity ~0.6% of the strongest perovskite peak is attributed to the pyrochlore phase which is a common impurity arising during the synthesis of PFN. Similarly weak peaks at ~27.5°, 28.4°, 30.6°, 32.4° and 33.1° indicate the presence of some other unidentified impurity phase(s) at low levels. Broadening and splitting of the perovskite 200 and 222 peaks closely similar to that shown in figure 3 of Majumder *et al* [45] was permissive of monoclinic lattice geometry but without the resolution needed for a definitive determination.

Another piece of the PFN pellet was polished for analysis in a Cameca SX-100 electron microprobe. X-ray maps for Fe, Nb and Pb showed variations in cation proportions, the extent of which is indicated by the results of 26 point analyses shown in figure 1. The average of these can be expressed in terms of 3 oxygen atoms or 2 cations as $Fe_{0.49}Nb_{0.49}Pb_{1.04}O_3$ and $Fe_{0.48}Nb_{0.49}Pb_{1.03}O_{2.97}$, respectively. Bright spots in the FeKα maps suggested the presence, in small proportion, of some iron-rich phase with dimensions below the spatial resolution of ~1 μm.

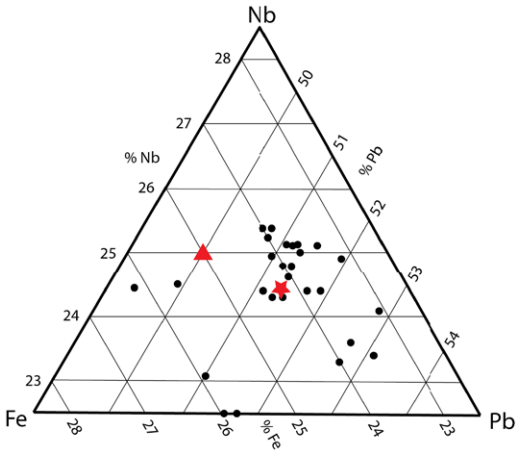

Figure 1. Cation proportions from individual electron microprobe analyses (wavelength dispersion, with respect to Fe_2SiO_4, Nb metal and PbS as standards). The triangle marks the ideal stoichiometry for PFN and the star is the average of 26 point analyses.

Dielectric data were collected using a QuadTech 7600 Precision LCR Meter at 1 kHz, 10 kHz, 100 kHz and 1 MHz, with an applied ac voltage of 1 V. Sample temperature was controlled in a Janis Cryocooler, with data collection during cooling from 450 to 10 K at 0.2 K min^{-1}. An average of 5 readings was obtained for each data point.

Magnetic properties of the RUS sample (mass 0.0500 g) and of a second sample (mass 0.013 43 g) were characterized in two different Quantum Design MPMS XL SQUID magnetometers, one in Cambridge (squid 1) and the other in Dresden (squid 2). Data were collected in low and high fields at low temperatures from both samples. High temperature data were collected in squid 2 with the second sample held in an open quartz tube.

A first order reversal curve (FORC) diagram was obtained at room temperature from the RUS sample using a Princeton Measurements Co. vibrating sample magnetometer manufactured by Lake Shore Cryotronics Inc., which is housed in the Nanopalaeomagnetism Lab at the University of Cambridge. This approach to characterization of magnetic samples is widely used in the context of rock magnetism, as introduced by Roberts *et al* [85] and Pike *et al* [86–88], and the complete FORC diagram is built up from many partial hysteresis curves, following Mayergoyz [89]. For the present study, a total of 325 FORCs were measured using a saturating field of 2.2 T, a field step of 6.75 mT, a time constant of 500 ms, and maximum coercivity (B_c) of 1.95 T. The FORCs were processed with the program FORCinel [90], using the VARIFORC method for variable smoothing [91]. Hysteresis loops were measured using a saturating field of 2.2 T, field steps of 5 mT, and a time constant of 200 ms. The saturation remanent magnetization, M_{rs}, was demagnetized by applying progressively increasing logarithmically spaced fields in the opposite direction to the

M_{rs}. The resulting backfield demagnetization curve (100 points in the interval 0.5 mT–2.2 T) was differentiated to obtain the coercivity spectrum, which was fitted with lognormal distributions representing the coercivity components.

Heat capacity was measured in a Quantum Design model 6000 PPMS with 6500 option controller. The sample had mass 0.025 39 g and was held in Apiezon H grease. Data were collected during heating from 3 to 396 K in 8 intervals of temperature, with step sizes of 1, 3 or 5 K, and a repeat data collection was made between 100 and 200 K. Each data point was an average of three measurements.

Resonant ultrasound spectroscopy (RUS) data were collected at room and low temperatures using equipment described elsewhere [92]. A rectangular parallelepiped with dimensions 4.650 × 2.160 × 0.666 mm^3 and mass 0.0500 g cut from the original disc was held lightly across its largest pair of faces between the piezoelectric transducers, and data were collected in 5 K steps from ~292 K to ~7 K and back up to ~292 K again, with 20 min allowed for thermal equilibration at each temperature. Individual spectra contained 65 000 data points in the frequency range 50–1200 kHz. The high temperature RUS instrument and associated experimental protocols have also been described elsewhere [93–95]. Temperature is measured with a thermocouple placed within a few mm of the sample but a small correction is then also applied, based on a calibration against the transition temperature of quartz. Two data sets were collected. The first was a heating and cooling sequence between ~296 and ~609 K with nominal steps of 5 K and 65 000 data points in the frequency range 100–1500 kHz. The second was a heating and cooling sequence through the temperature interval ~316–399 K, with nominal steps of 2 K and 65 000 data points in the frequency range 100–1200 kHz. In both cases a 20 min settle time was allowed for thermal equilibration at each set point. The primary spectra were all analysed offline using the software package IGOR (Wavemetrics). Selected peaks were fit with an asymmetric Lorentzian function to give their frequency, f, and width at half maximum height, Δf. f^2 scales with the elastic modulus that determines the particular resonance mode and for most modes this is dominated by the shear modulus. The inverse mechanical quality factor, Q^{-1}, is a measure of acoustic loss and is given by $\Delta f/f$.

3. Results

Data for the real part of the dielectric constant, ε', and the dielectric loss, tanδ, are given in figure 2. There is a very obvious shoulder in both ε' and tanδ at ~360 K, independent of frequency, which coincides with the expected temperature of the tetragonal–monoclinic transition. A broad peak occurs in ε' has its maximum at ~389 K when measured at 1 MHz, which is within the range expected for the cubic–tetragonal transition. However, significantly greater values of ε' are observed at lower frequencies and the maxima shift to higher temperatures when measured at 10 kHz and 100 kHz, i.e. ~426 K and ~429 K respectively. There is a break in slope at ~423 K in the data measured at 1 kHz. Tanδ values are highest

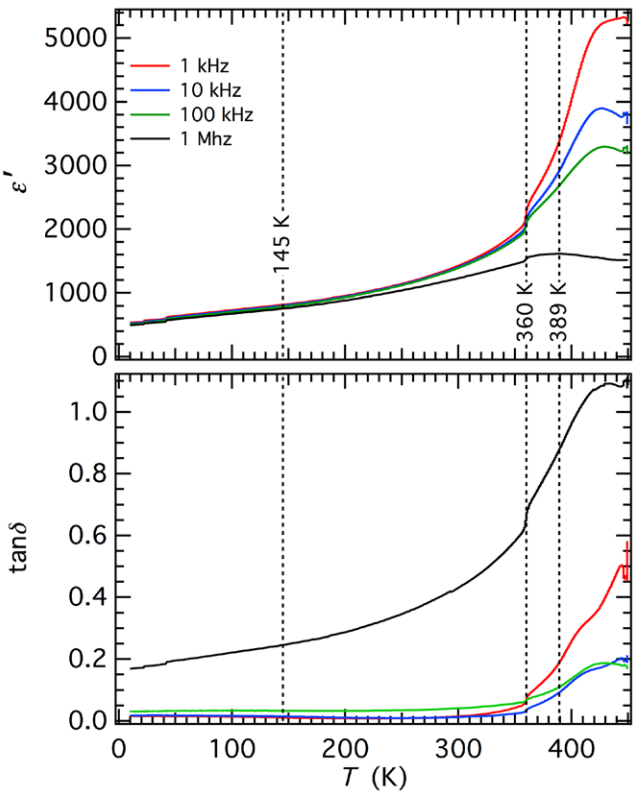

Figure 2. Variations with temperature of the dielectric constant, ε', and dielectric loss, tanδ, for PFN, as measured at four different frequencies during heating from 10 to 450 K at 0.2 K min^{-1}.

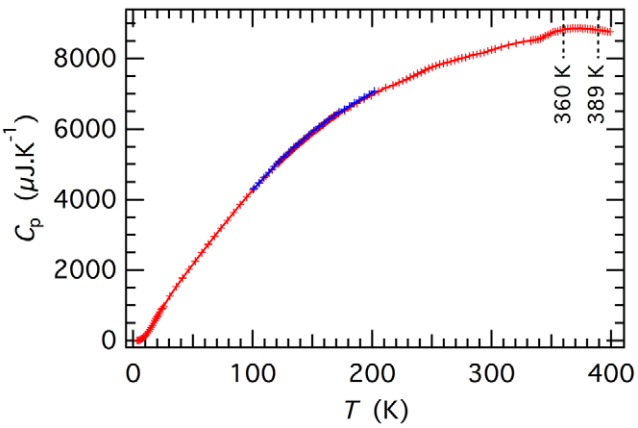

Figure 3. The heat capacity as a function of temperature does not appear to show any anomaly in the vicinity of the expected Néel point, ~140–150 K. There is a broad excess above ~340 K which reaches a maximum at ~375 K.

when measured at 1 MHz and have a broad maximum centred at ~432 K. Values measured at lower frequencies are substantially lower over the entire temperature range and increase steeply above the step at ~360 K. The 100 kHz data have a broad peak centred at ~430 K. This pattern is not typical of a relaxor which would be expected to show frequency dependent maxima, with the peaks in ε' and tanδ occurring at progressively higher temperatures with increasing frequency.

The variation of heat capacity, C_p, between 3 and 399 K is shown in figure 3. Notably, there is no anomaly detectable in

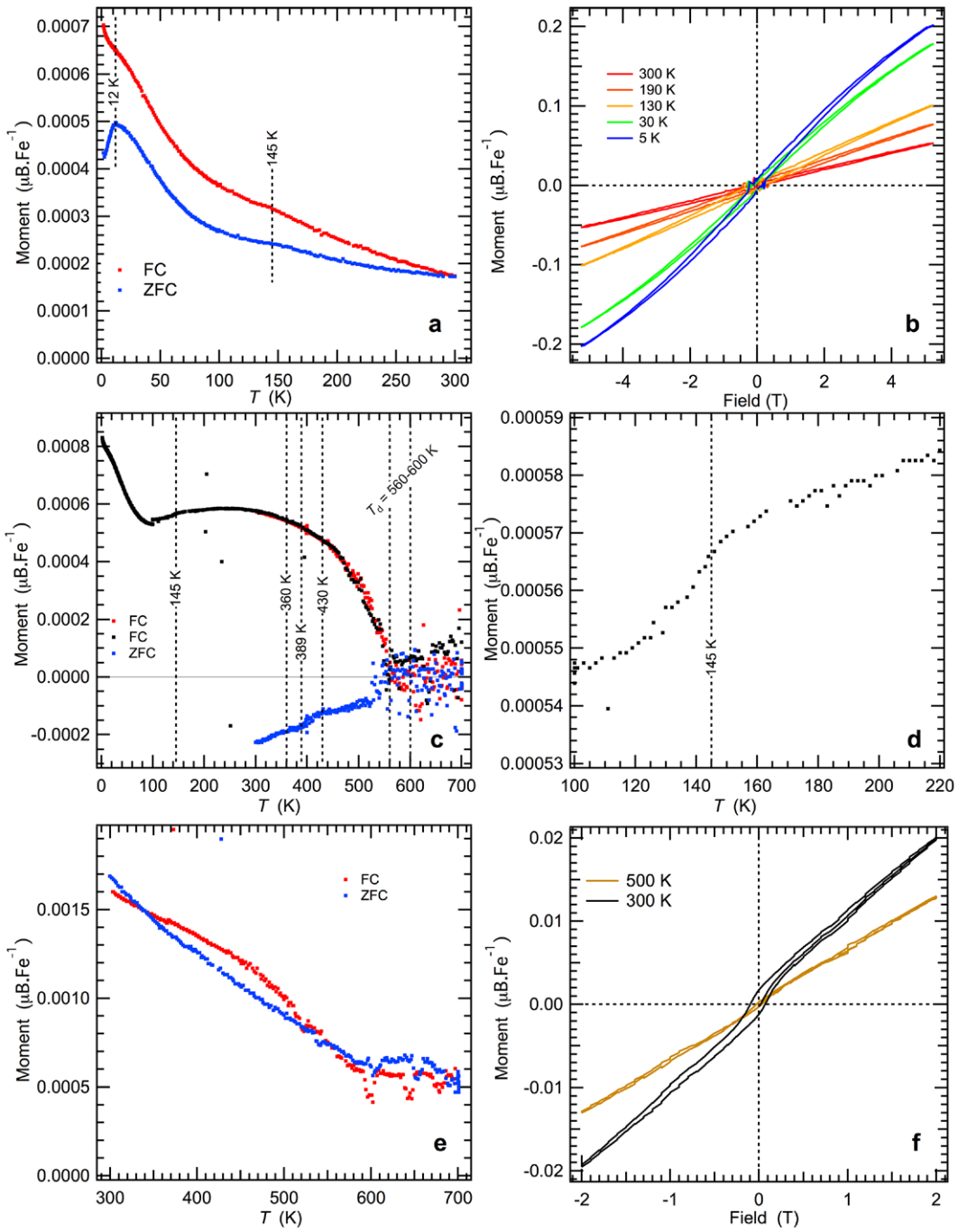

Figure 4. Magnetic data for PFN. (a) Squid 2. Magnetic moment measured during heating in an applied field of 0.01 T, following cooling in zero field (ZFC) and then following cooling in the 0.01 T field (FC). (b) Squid 1. Hysteresis loops collected from the RUS sample; individual data sets at each temperature were collected in a cooling sequence. (c) Squid 1. Data labelled ZFC were collected during heating with an applied field of 0.01 T following cooling in the nominally zero field of the instrument. Two sets of data, labelled FC, were collected in cooling sequences from 700 to 300 K and from 700 to 2 K in an applied field of 0.01 T. (The very small step at ~100 K is an artefact, arising from the way the data were collected). (d) Closer view of the FC data shown in (c), showing the very slight anomaly in the vicinity of 145 K. (e) Squid 2. ZFC data collected in a field of 0.1 T during heating, following cooling in the nominally zero field of the instrument. FC data collected during cooling in a field of 0.1 T. (f) Squid 2. Hysteresis loops measured at 300 and 500 K.

the vicinity of the expected Néel point. A broad excess heat capacity is clearly present above ~340 K but the data do not extend to high enough temperatures to see where this would end. The maximum occurs at ~375 K and there does not seem to be evidence for distinct peaks either at ~360 or ~389 K.

Figure 4(a) shows magnetic moments measured with an applied field of 0.01 T in squid 2 during heating from 2 to 300 K. The data set labelled ZFC was collected following cooling in zero field and the data set labelled FC following cooling in the 0.01 T field. The resulting variations in moment with temperature are closely similar to what has been reported in other studies for a variety of fields (e.g. [21, 26, 31, 40, 41, 50, 59, 96, 97]). Specifically, there is an anomaly in the vicinity of 145 K which has elsewhere been attributed to

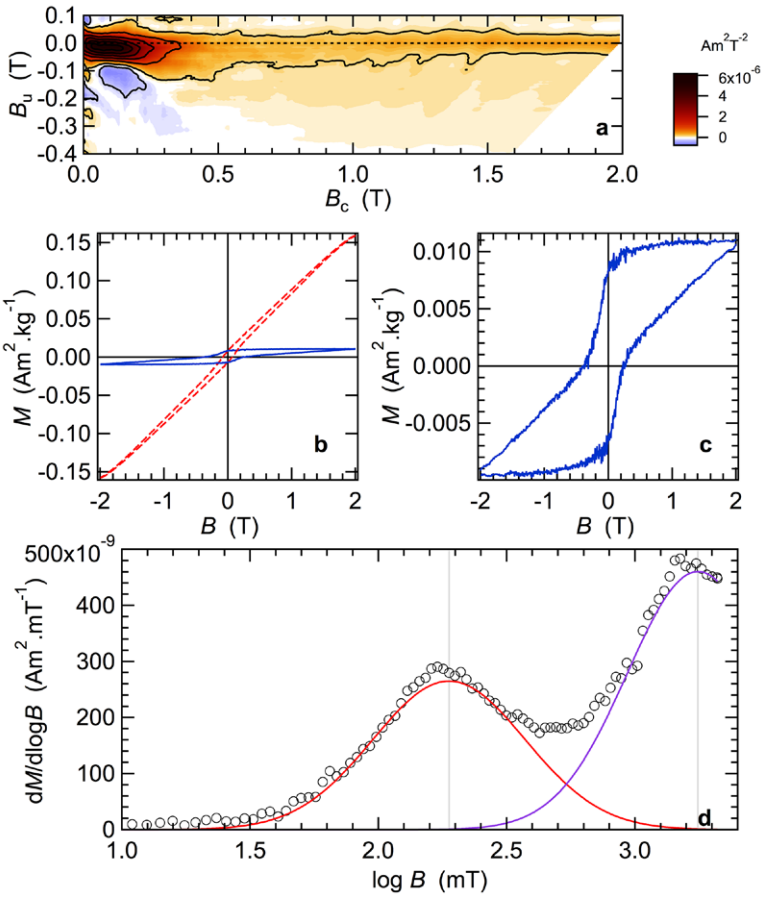

Figure 5. (a) Room temperature FORC diagram with areas of positive (red) and negative (blue) regions: the strong positive feature at low values of B_u and B_c implies the presence of a ferromagnetic component with low coercivity and the weaker feature extending out to high values of B_c implies the presence of a second component with high coercivity. Both components are statistically significant. (b) The raw hysteresis loop (red intermittent line) has been corrected for paramagnetic contributions by subtracting the high field susceptibility to give the blue curve. (c) Blue curve from (b) at larger scale showing a wasp-waisted ferromagnetic hysteresis loop. (d) Coercivity component fitting of the backfield demagnetization curve. The area under each curve is proportional to the magnetization held by each component. Component 1: median coercivity = 0.19 T, estimated contribution to remanence ~25%; component 2: median coercivity 1.76 T, estimated contribution to remanence ~75%.

antiferromagnetic ordering, though this is somewhat smaller for the present sample. The cusp with a maximum at ~12 K in the ZFC data has been attributed to the influence of the spin glass transition. Magnetic hysteresis curves collected from the RUS sample at 300, 190, 130, 30 and 5 K in a cooling sequence, with applied fields between +5 and −5 T in squid 1, are shown in figure 4(b). They show a small opening and confirm a ferromagnetic ordering component in the sample at all five temperatures. Some curvature at high fields in the 5 and 30 K loops is indicative of a tendency to approach saturation but no evidence for saturation was observed at 130, 190 and 300 K. The lower temperature data also show slightly wider loop openings than at higher temperatures.

Figure 4(c) is a compilation of data from the high temperature instrument (squid 2, second sample). In this case, the magnetic moment was measured during heating from 300 to 700 K in a field of 0.01 T, following cooling from 700 K in the nominally zero field of the instrument (labelled ZFC). The two sets of data labelled FC were collected in an applied field of 0.01 T during cooling in stages from 700 to 300 K and from 700 to 2 K. These show that the moment goes to zero at ~560 K, which is referred to here as T_{cFM}. The opposite sign of the measured moment between the ZFC and FC sets implies poling in the nominally zero field of the instrument, which must have actually been non-zero and slightly negative, as the sample was cooled through the ferromagnetic transition. There is a small change in slope at 460 K in the FC datasets; the trend of increasing moment with falling temperature subsequently levels off and then reverses at ~240 K. Figure 4(d) shows the FC data between 100 and 220 K at higher magnification, and reveals that there is only a subtle change in slope at the expected Néel point of ~145 K. Finally, the relatively steep increase in moment below ~100 K becomes even steeper below ~5 K. Temperatures of known structural changes have been added to figure 4(c) for comparison. T_{cFM} is close to the range of temperatures estimated for T_d (~560–600 K) from Dul'kin *et al* [12], and there are slight changes in slope of the ZFC data in the vicinity of 430 and 389 K, corresponding with values of T^* and T_c, respectively, deduced from other measurements.

Data collected during heating from 300 to 700 K in a field of 0.1 T, following cooling in the nominally zero field

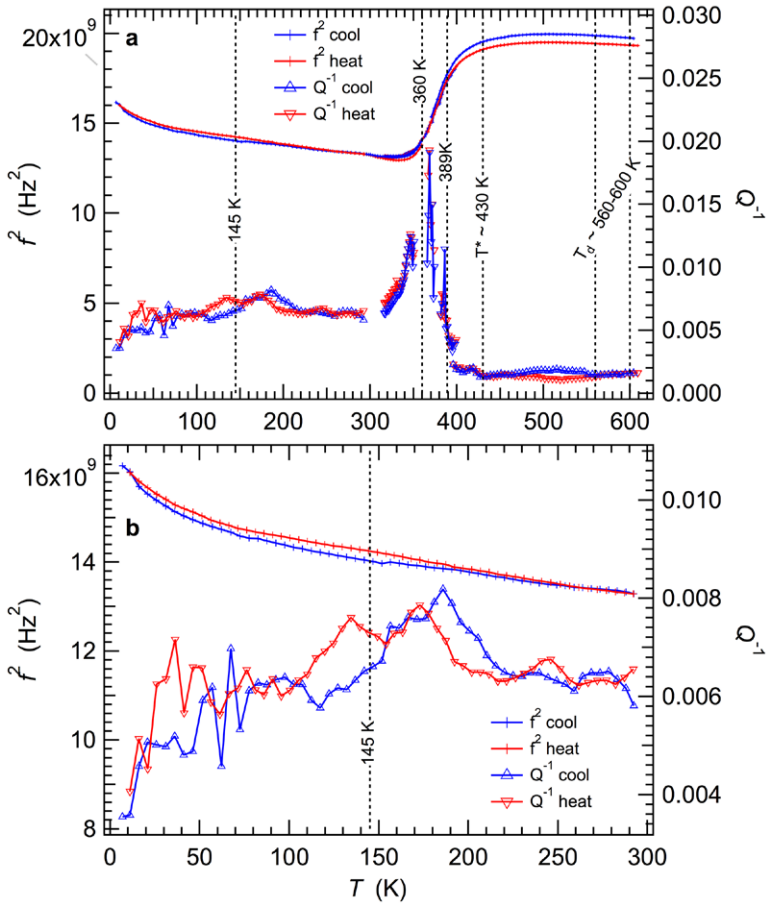

Figure 6. RUS data for PFN. (a) f^2 and Q^{-1} from fitting of selected resonance peak and combining the data from one peak in the low temperature data set and three different peaks from the high temperature data sets. Frequencies of the high temperature data sets have been rescaled so that they have the same values as the low temperature data set at room temperature. (b) Detail of results below room temperature for the resonance peak with $f = 115$ kHz at 292 K.

of the instrument (labelled ZFC) are shown in figure 4(e). Data collected with an applied field of 0.1 T during cooling (labelled FC) are also shown. The moments have the same sign and magnitude, indicating that a 0.1 T field is sufficient to induce poling at 300 K. The slope goes to zero at ~590 K, indicating a field shift for T_{cFM} of ~30 K. Hysteresis curves measured between +2 and −2 T at 300 and 500 K are shown in figure 4(f). These were collected with the magnetometer in persistent mode by first heating to 600 K and then cooling to the set temperature in nominally zero field. The loops remained open, consistent with the view that the sample is weakly ferromagnetic.

Figure 5 shows the results of the room temperature FORC analysis, which are interpreted in terms of the presence of two magnetic components. The FORC diagram itself (figure 5(a)), with B_c as coercivity field and B_u as bias field (relating to local interaction fields), has two main features, both passing a statistical significance test [98]. The low coercivity component implied by the strong maximum at low values of B_u and B_c, vertical spreading, together with the pairing of the stronger positive (red–black) and weaker negative (blue) areas and the displacement below the horizontal axis, is indicative of discrete particles consisting of single magnetic domains with inter-particle magnetostatic interactions that are creating a net positive mean interaction field. The weaker feature centred on $B_u = 0$ which extends to high values of B_c is indicative of a magnetic component with high coercivity. In figure 5(b), the raw hysteresis loop (red intermittent line) was corrected (blue line) for paramagnetic contributions by subtracting the high field susceptibility. The resulting ferromagnetic hysteresis loop (figure 5(c)) exhibits wasp-waisting (constriction), characteristic of a bimodal mixture of high and low coercivity components. Coercivity component fitting of the back-field demagnetization curve results in the curves shown in figure 5(d). The area under each curve is proportional to the magnetization held by each component.

Results from the RUS measurements are given in figure 6 in the form of f^2 and Q^{-1} values obtained by fitting selected resonance peaks. It was not possible to follow a single peak through the entire temperature range between 7 and 609 K, but it has been possible to combine results from different peaks to show the overall pattern of elastic softening and acoustic loss (figure 6(a)). The frequency at room temperature of the peak from the low temperature spectra was 115 kHz. Experience has shown that there are small differences in the absolute values of resonance frequencies and peak widths between the low T and high T RUS instruments, due to the influence of the alumina buffer rods required to access high temperatures, but the

resonances are still determined predominantly by shear modes. Data from the high temperature instrument are composite from three peaks, to which scaling factors have been applied so as to match them up with the low temperature data. These had $f \sim 242$ kHz, ~254 kHz and ~136 kHz at room temperature. The most striking overall feature is the marked reduction of f^2, by ~30–35%, with falling temperature between ~430 and ~330 K. This corresponds with elastic softening predominantly of the shear modulus and is clearly related to the ferroelectric transition. The onset of precursor softening occurs in the vicinity of ~550 K, close to $T_d \sim 560$–600 K reported by Dul'kin *et al* [12]. The minimum in f^2 values occurs at ~330 K and there is then a return to the normal trend of elastic stiffening with falling temperature. This would be expected to level off to a slope of zero as $T \rightarrow 0$ K but instead the trend below ~85 K is of increasing stiffness.

At ~0.001–0.002, Q^{-1} values are relatively low between ~609 and ~430 K and are not dissimilar from other synthetic polycrystalline samples of cubic perovskite (e.g. $SrZrO_3$ [99], $BaCeO_3$ [94], $Pr_{0.48}Ca_{0.52}MnO_3$ [100], $PbMg_{1/3}Nb_{2/3}O_3$ (PMN) [95], $PbSc_{0.5}Ta_{0.5}O_3$ (PST) [101], $0.26Pb(In_{1/2}Nb_{1/2})O_3$ –$0.44Pb(Mn_{1/3}Nb_{2/3})O_3$–$0.30PbTiO_3$ [102], $BaTiO_3$ [103]). There is a distinct but small increase in the acoustic loss below ~425 K, coincident with the value of T^* given by Dul'kin *et al* [12], and then a much steeper increase below ~395 K which is close to the expected value of T_c for the cubic–tetragonal transition. Between ~350 and ~370 K the resonance peaks became so broad that it was not possible to determine line widths. This interval of high Q^{-1} coincides with the transition temperature of ~360 K evident in the dielectric data and taken to correspond to the tetragonal–monoclinic transition. Below the peak in Q^{-1} between ~395 and ~320 K there is a plateau of relatively high values which only start to reduce below ~85 K in correlation with the increasing values of f^2. Finally, it is notable that if there are anomalies in f^2 and Q^{-1} near T_N, they are at the level of or smaller than noise in the data.

Details of the variations of f^2 and Q^{-1} below room temperature are shown in figure 6(b). Differences between heating and cooling are small but are greater than the expected instrumental resolution. There are weak peaks in Q^{-1} at ~185 K during cooling and at ~135 and 170 K during heating. Obvious noise in the data below ~80 K is due to the fact that the resonance peaks became progressively weaker at the lowest temperatures. Even at this level of detail, there appear to be no features which occur specifically at ~145 K.

4. Discussion

4.1. Transformation sequence

Wide variations in physical properties have already been recorded for PFN samples prepared in different ways (e.g. [75]), so it should not be surprising that those of the sample used in the present study also have differences. In particular, the dielectric data do not quite match with the more typically observed properties indicative of a ferroelectric transition with $T_c \approx 385$ K. Rather than having a frequency-independent maximum, the dielectric constant has a maximum at about the expected temperature when measured at 1 MHz but then a frequency dependent maximum in the vicinity of 430 K when measured at lower frequencies (figure 2). Instead of the relatively sharp lambda anomaly in C_p at ~375 K reported by Bhat *et al* [13], a broad anomaly has been observed implying that there is some smeared out contribution to the ferroelectric transitions. The conventionally measured magnetic properties (figure 4(a)) appear to be rather similar to those reported in other studies but the peak in heat capacity which would be expected to accompany a conventional antiferromagnetic ordering transition is notably absent. Moreover, the present sample is weakly ferromagnetic up to 560 K, while evidence for the antiferromagnetic transition at ~145 K is only a subtle change in slope of magnetic moment as a function of temperature rather than a maximum. The magnetic data show similar anomalies at low temperatures to those which have been ascribed to the spin glass transition, but any associated anomalies in either heat capacity or dielectric properties are at or below the limit of resolution of the data given in figures 3 and 4.

Because of the diffraction evidence for the presence of impurities at the level of ~1%, the possibility remains that the weak ferromagnetism is not due to PFN itself. Speckles in the x-ray maps from electron microprobe analysis suggest that at least one of the impurity phases could be iron rich, and the most obvious candidate is unreacted or partially reacted Fe_2O_3 which persisted through the synthesis process. At room temperature α-Fe_2O_3, hematite, has a weakly ferromagnetic (canted antiferromagnetic) structure. The lower coercivity component recognized from the FORC analysis contains ~25% of the total remanence of the sample and, using a value of 0.5 A m^2 kg^{-1} for the saturation magnetization, this could be accounted for by 0.5% by mass of hematite. However, the Néel point of hematite is ~955 K and it typically has a second magnetic transition, the Morin transition, at ~250–260 K which is not evident in any of the data in figure 4. The Morin transition becomes suppressed to lower temperatures with reducing grain size [104], so that the low coercivity component still could be due to a fine dispersion of hematite on grain boundaries. Another possibility is ε-Fe_2O_3, which exists only in nanocrystalline form, is ferrimagnetic with a Curie temperature of ~510 K, and has a high room temperature coercivity of ~2 T [105–109]. This material might account for the high coercivity component of the PFN sample except that it has an additional magnetic transition at ~100 K, marked by a steep drop in magnetization [107–109] that is not seen in the data in figure 4. Other possibilities include $Pb_2Fe_2O_5$, for example, which is weakly ferromagnetic up to 520 K. However, the moment in a 0.1 T field reported for 400 K by Gil *et al* [110] is only similar in magnitude to that found for the entire sample of PFN. If the weak ferromagnetism is due to an impurity, the same impurity would presumably be responsible for the similar overall ferromagnetic behaviour below ~530 K reported by Fraygola *et al* [46] for both PFN and PFW ($Pb(Fe_{2/3}W_{1/3})O_3$).

There is independent evidence that the antiferromagnetic transition is suppressed in some samples of PFN. Instead of the classical pattern of reducing intensity to zero at $T_N \sim 160$ K

of the magnetic superlattice reflection in neutron single crystal diffraction observed by Howes *et al* [25] and Chillal *et al* [26], Stock *et al* [24] found only short range ordering with the length scale of magnetic correlations increasing from ~10 Å at the highest temperatures to ~17 Å at the lowest temperatures. Their magnetic data collected in a 0.01 T field do not seem to show any anomaly in the vicinity of 150 K. The sample of Yang *et al* [54] did not have a heat capacity anomaly in the vicinity of ~150 K, in spite of there being a slight anomaly in magnetic moment (measured at 0.1 mT) associated with antiferromagnetic ordering. Their dielectric data are rather similar to those reported here in having a clear frequency-independent anomaly at ~360 K and a peak at ~375 K when measured at 1 MHz; at 10^4 and 10^5Hz the dielectric constant increased at higher temperatures. On the basis of Mössbauer data Yang *et al* [33, 52] concluded that antiferromagnetic ordering below ~143 K was accompanied by the development of a ferromagnetic component. Dielectric data collected in the vicinity of 150 K, however, are quite different from the smooth variation seen in the present study, in that their data have sharp steps in both ϵ' and $\tan\delta$ [33].

The most likely causes of variations in intrinsic dielectric and magnetic properties of PFN are variations in the degree of local ordering of Nb and Fe ions on crystallographically distinct B-sites. Larger domains of atomic order would be expected to result in larger PNRs and conventional antiferromagnetic ordering with $T_N \sim 143$ K, while smaller clusters would give rise to smaller PNRs and suppression of the antiferromagnetic order. On this basis, the present sample is likely to be towards the more disordered end of the scale. The dielectric data are permissive of the expected ferroelectric transitions in the vicinity of 385 K and then to a different ferroelectric structure at ~360 K, but with a relatively high contribution from relaxor behaviour. The heat capacity anomaly has a form which is more like that for PMN or PFT [111] than for a conventional ferroelectric transition. With regard to the magnetic transitions, the high coercivity ferromagnetic component must arise from spin clustering of some kind related to the relatively disordered local distribution of Fe and Nb if it is intrinsic to the PFN. Suppression of the antiferromagnetic transition near 150 K could be a consequence of the effect of reducing grain size [71], but there is no evidence in the diffraction data from the present sample that the grain sizes are unusually small. It is therefore presumed to be a consequence, also, of a relatively high degree of cation disorder in the sample. Variations of the magnetic moments at the lowest temperatures imply that the spin glass behaviour of the present sample is similar to that reported in the literature.

4.2. Strain/order parameter coupling

The elastic properties of PFN are dominated by 30–35% softening of the shear modulus which is clearly associated with the ferroelectric/structural transitions in the vicinity of 350–395 K. The pattern of softening is typical of the effects of coupling of the driving order parameter with shear strain, as is well understood for phase transitions in many other single crystal and polycrystalline materials (e.g. [112–114]). An applied stress induces a lattice strain which, in turn results in a relaxation of the order parameter, due to the strain/order parameter coupling, so that the measured elastic constant is softer than would be the case if there was no phase transition. In this context the first requirement is to determine the form and magnitude of the macroscopic strain. As set out in the appendix, this has been done for PFN using published data for lattice parameters or thermal expansion (figure A1(a)) [7, 16, 18, 56, 74]. There is one non-zero shear strain for each of the tetragonal and rhombohedral structures and three for the monoclinic structure, the magnitudes of which vary up to ~4‰ (figure A1(c)). Each of these is expected to scale with the square of some component(s) of the driving order parameter. Based on strains determined from the data of Ehses and Schmid [7], the cubic–tetragonal transition must be close to tricritical in character, i.e. $q^4 \propto (T_c - T)$ (figure A1(d)). The shear strain of the rhombohedral structure and two of the shear strains of the monoclinic structure show similar dependences though the values of T_c which their extrapolation to zero would imply are not the same. If there was only one instability and the different structures are simply due to changes in the lowest energy orientation of the ferroelectric polarization, a single T_c in the vicinity of 385 K should be observed. More tellingly, the shear strains should then also scale with each other and extrapolate to a common origin. That this is not the case (figure A1(b), strains calculated from the data of Singh *et al* [18]) implies that the monoclinic structure owes its stability to a combination of two separate order parameters. The first is likely to be a soft optic mode with symmetry properties of irreducible representation Γ_4^-, responsible for the ferroelectric transition, but the origin of a second order parameter is not known. One possibility, considered by Scott [115] for PFN–PZT, is that the second order parameter is magnetic, with symmetry such that strain coupling induces the monoclinic distortion.

The second important result of the strain analysis is that there is no detectable shear strain in the vicinity of T_N. Thus, even if there was a relatively normal antiferromagnetic transition in the present sample, it would not be expected to give rise to an anomaly in the temperature dependence of the shear modulus (unless there were contributions from biquadratic coupling between the magnetic order parameter and strain). On the other hand, there is a small volume strain of up to −1‰ at ~150 K (figure A2(b)), which is opposite in sign to and substantially smaller than the volume strain which accompanies the ferroelectric/structural transition. A small anomaly would be expected to occur in the bulk modulus as a consequence of this coupling, but would not be expected to be seen in the temperature dependence of resonance modes which are dominated by shearing in an RUS experiment. The only hints of possible magnetoelastic coupling in the RUS data are the small peaks in Q^{-1} between ~120 and ~200 K but they are different between heating and cooling.

In detail, the RUS data are consistent with an onset of precursor softening occurring in the same temperature range, ~560–600 K, as that in which acoustic emission occurs and has been

used to infer the first appearance of dynamical PNRs [12]. The same onset of softening at T_d was found in PMN [95] and PST [101]. It is probably typical of relaxor-like behaviour, though it also precedes more conventional ferroelectric transitions, as in $BaTiO_3$ [103]. The small increase in acoustic loss below ~425 K correlates with T^*, the temperature at which acoustic emission was taken by Dul'kin *et al* [12] to imply that the PNRs acquire some static or quasi-static aspect. Some part of the microstructure, either walls between the PNRs or twin walls within them must have ferroelastic character such that it moves under the influence of an external stress on the time scale of the measurement. The form of this microstructure has not been established but could be a tweed pattern, as has been proposed ahead of the ferroelastic/ferroelectric transition in PST [101] and ahead of the ferroelastic/ferrimagnetic transition in $ErCo_2$ [116].

The variation of f^2 through the transition interval does not give any indication that there are two ferroelectric/structural transitions in the sample used in the present study but the steep increase in Q^{-1} starts at ~395 K and the interval in which the resonance peaks become particularly broad is centred on ~360 K. These temperatures correlate with the acoustic emission results reported by Dul'kin *et al* [12] for transitions at ~348–363 K and ~365–382 K. At least part of the contribution to the acoustic loss could come from movement of interfaces between monoclinic and tetragonal domains in a temperature interval of two coexisting phases, but the dominant loss mechanism is likely to be due to the mobility of ferroelastic twin walls or tweed under the influence of external stress.

The plateau of relatively high acoustic loss between ~300 and ~50 K is due to the dynamic properties of whatever microstructure that arises as a consequence of the ferroelastic aspects of the ferroelectric phase transitions. In the vicinity of a second order transition, the number density, N, and thickness, w, of ferroelastic twin walls are expected to vary as $w \propto N \propto (T_c - T)^{-1}$ as $T \rightarrow T_c$ [117–120]. Viscous drag on the twin walls due to interaction with the underlying lattice and point defects is greater for thin walls than thick walls [121, 122], and thick, widely spaced walls immediately below T_c give rise to smaller loss than at lower temperatures where they become thinner and more numerous. The actual mechanism for lateral motion of the walls at RUS frequencies is most likely due to lateral motion of ledges within the walls [123–125] and, below some temperature interval, this motion becomes frozen by pinning to defects. The typical pattern of acoustic loss with falling temperature below a ferroelastic transition is therefore first a steep increase starting at ~T_c, followed by a plateau of high values related to the viscous drag. This is then followed by a frequency dependent Debye loss peak due to the freezing process, below which the acoustic loss returns to more or less the same low level as occurs in the para phase above T_c. One example of this pattern is shown by the cubic–rhombohedral octahedral tilting transition in $LaAlO_3$ [126, 127] and another is for the cubic–tetragonal–\rhombohedral ferroelectric transitions in $0.26Pb(In_{1/2}Nb_{1/2})O_3$–$0.44Pb(Mn_{1/3}Nb_{2/3})O_3$–$0.30PbTiO_3$ [102]. The pattern observed here for PFN differs from this model, in that there is neither a Debye loss peak nor a return to low values of Q^{-1} that would signify freezing of the twin wall motion due to pinning by one type of point defect. Rather, there is a suggestion in the data shown in figure 6(b) that the plateau region contains of a series of overlapping Debye peaks, signifying freezing of motion of a succession of different defects with different relaxation times. This is more similar to the loss behaviour of PMN [95], in which the acoustic properties are dominated by the static and dynamical behaviour of PNRs, and is also consistent with the tweed microstructure reported to be stable from T_c down to at least ~110 K in PFN [79]. Instead of there being discrete and highly mobile twin walls, as in $LaAlO_3$, heterogeneous strains due to the underlying chemical and structural heterogeneity become self-organized in a pattern of intersecting strain modulations. In the terminology of Viehland and Salje [128] this is an 'adaptive' structure in which the properties of the crystal become dominated by a combination of both the domains and the domain walls rather than simply by some relatively small number of discrete domain walls. Acoustic losses must arise from local adjustments of different parts of the microstructure under stress and the freezing process will occur by pinning mechanisms that have a wider range of thermal barriers and relaxation times. Instead of the classic Debye loss peak and elastic stiffening associated with a single freezing mechanism, there will effectively be a wide spread of smaller, overlapping loss peaks and a corresponding gradual increase in stiffness with falling temperature.

The RUS data presented are similar to other data for the elastic properties of ceramic PFN in showing large changes in compliance or moduli in the vicinity of 350–400 K [37, 56, 58, 63, 80, 81], ~430–470 K [81] or ~300–430 K [82]. The slightly different temperature intervals are presumed to be simply due to variations in the ferroelectric transition temperatures between samples. Pulse-echo ultrasonic measurements at 10 MHz also revealed additional small anomalies in elastic constants at ~110, ~170 and ~250 K amounting to abrupt stiffening or softening by up to 0.5% [37, 58, 63, 80] in a sample with $T_N \approx 170$ K. The overall pattern of acoustic loss accompanying these appears to be a series of Debye peaks at the same temperatures [37, 58]. Acoustic loss associated with measurements of Young's modulus at ~800 Hz shows a small peak at T_N [81]. The overall picture is thus of variations between different samples but all showing strong strain coupling with ferroelectric order parameters, weak coupling with antiferromagnetic ordering and the existence of strain relaxation processes across the entire stability field of the monoclinic structure. Observation of differences between cooling and heating (figure 6, and see [63]) indicate a dependence on thermal history that is most likely due to changes of microstructure. For example, Meng *et al* [79] reported a hysteresis for the presence of wedge shaped domains containing different configurations of tweed microstructure on cooling below ~120 K. If the proportions of such domains change to produce even a small change in elastic anisotropy of the sample as a whole, this will be seen as a hysteresis in the resonance frequencies.

4.3. Contrasting dielectric and acoustic loss behaviour

In a conventional ferroelectric material which is also ferroelastic, strong coupling between the ferroelectric order

parameter and symmetry breaking shear strain should ensure that the response to externally applied electric or stress fields will be qualitatively similar. For a relaxor such as PMN, the dielectric and strain relaxation properties differ in some details but their variation through the freezing interval is still qualitatively the same [95]. By way of contrast, dielectric data for PFN in the literature show a wide range of patterns of variation and the dielectric data for the sample used in the present study (figure 2) are substantially different from the elasticity data (figure 6). This appears to be a reflection of two factors, the variability of samples according to how they were synthesized and the existence of additional dielectric loss mechanisms relating to electrical conductivity. Some of the wide variability between samples is illustrated, for example, in [129–131]. A 'typical' pattern is of a broad maximum in ε' centred on the ferroelectric transition point, with a frequency dependent tail to high temperatures, and tanδ showing a frequency dependent increase with increasing temperature above T_c [37, 50, 57, 59, 132]. Above the transition point the dielectric constant and the dielectric loss reduce with increasing frequency. This part of the dielectric behaviour is attributed to the contribution of conductivity (e.g. [50, 57]).

The sample used in the present study is 'typical' in having a frequency dependent increase in dielectric loss above T_c but this does not appear in the acoustic loss. The 1 MHz dielectric data should exclude the influence of conductivity and ε' shows the two ferroelectric/structural transitions as a step at ~360 K and a peak at ~389 K. Peaks appear in both ε' and tanδ in the vicinity of 430 K at some frequencies, however. These coincide with T^* and the increase in Q^{-1}, suggesting that partial freezing of PNRs is being detected in both data sets. On this basis, the high dielectric loss at 1 MHz is presumed to relate to purely ferroelectric aspects of PFN (as apposed to contributions from conductivity). The high dielectric and acoustic losses below T_c can both be understood in terms of mobility of defects within a complex microstructure.

4.4. Local strain heterogeneity and magnetic ordering

Evidence from NMR spectroscopy points to the view that 'at nanoscale PFN is a chemically and magnetically inhomogeneously disordered system' [71]. On a mesoscopic length scale of ~10–50 nm, PFN can also have a domain pattern with variable dielectric constant at room temperature [133] and tweed microstructures across a wide temperature interval [79]. Some idea of the likely complexities of possible microstructures, more generally, can been seen in $Pb(Fe_{0.5}Ta_{0.5})_{0.4}(Zr_{0.53}Ti_{0.47})_{0.6}O_3$ [5, 115]. Any cation ordering which developed during the synthesis process must give rise to clusters with differences in charge distribution between their centres and boundaries. PNRs retained through the ferroelectric transitions will have variations in local polarization at their boundaries and across domain walls within them, and these may be coupled with ferroelastic strains. There will also be twin walls with gradients of both ferroelastic strain and ferroelectric polarization or just polarization alone, due to the macroscopic changes in symmetry from cubic to tetragonal, rhombohedral or monoclinic. Below T_N there will be antiphase boundaries, not coupled with shear strains, between domains with antiferromagnetic order. If long range antiferromagnetic ordering does not develop, there will be clusters with local magnetic order and if ferromagnetism develops at high temperatures there will be magnetic domain walls which could also have some ferroelastic character, depending on the symmetry of the ferromagnetic structure. Each of these components of the total microstructure involves inhomogeneities in the relevant order parameters and they must be coupled with inhomogeneities in other order parameters if, as is believed to be the case, there is magnetoelectric coupling in the system.

Some resolution of the local heterogeneity from the perspective of ferroelastic microstructures seems to occur by self organization in the form of tweed. The plateau of relatively high acoustic loss below ~320 K can then be understood as being the integration of contributions from adjustments of the locally strained regions instead of from the motion of discrete ferroelastic twin walls. As already suggested above, the gradual decrease in Q^{-1} and corresponding increase in f^2 below ~85 K in turn signifies freezing of this relaxation behaviour due to pinning by defects with some spread of relaxation times. The same loss pattern seen in $Pb(Fe_{0.5}Ta_{0.5})_{0.4}(Zr_{0.53}Ti_{0.47})_{0.6}O_3$ was attributed more directly to the influence of antiferromagnetic ordering or some other transition [3], but a rather similar trend has now been seen also in RUS data from $Pb_{0.4}Zr_{0.6}TiO_3$ (Schiemer, unpublished results). Since PZT does not have magnetic transitions, it is likely that this particular pattern of elastic stiffening and anelastic loss at low temperatures is essentially ferroelastic in origin. The magnetic ordering transitions of PFN occur within a material which thus has chemical heterogeneity at the atomic scale plus self-organized strain heterogeneity coupled with ferroelectric ordering on a mesoscopic scale.

If there is any strain coupling with the magnetic order parameters, it is inevitable that the local strains would act as fields, imposing some additional constraints on how the magnetic structures develop. Volume strains accompanying the antiferromagnetic and ferroelectric transitions are negative and positive, respectively, and because of this opposite sign, coupling via a common strain mechanism should be unfavourable. In other words, the antiferromagnetic and ferroelectric order parameters should act to suppress each other. At least in the present sample, there seems to be a correlation between increased relaxor characteristics and changes in magnetic properties. Most notably, the onset temperature of 530–580 K for ferromagnetism reported by Fraygola *et al* [46] and $T_{cFM} \approx 560$ K determined here coincides with the temperature, T_d, at which dynamical PNRs first appear. If it is intrinsic and the correlation between T_d and T_{cFM} is not mere coincidence, the origin of ferromagnetism in PFN could be dependent on the size, structure and dynamics of the PNRs together with the accompanying strain variations. Evidence from inelastic neutron scattering also points to magnetoelectric coupling in the dynamical regime [24]. Consideration of superantiferromagnetic or superparamagnetic clusters related to the PNRs would be one approach for explaining the ferromagnetic signal but

there is also a ferrimagnetic structure close by in the energy landscape of PFN [77, 78]. On the basis that there is some degree of magnetoelectric coupling via common strains, the onset of spin glass like behaviour below ~100 K would be related to freezing of strain relaxations arising from defects due specifically to the ferroelastic and ferroelectric history of the sample.

5. Conclusions

The RUS results highlight ferroelastic aspects of the structural phase transitions and transformation microstructures of PFN. In particular:

(i) There is classical coupling of the structural/ferroelectric order parameter with strain that gives rise to substantial softening of the shear modulus through the temperature interval ~350–420 K.
(ii) The two characteristic temperatures, T_d and T^*, associated with the development of PNRs are marked by the onset of elastic softening and a slight increase in acoustic loss, respectively, confirming that the local polarizations involved are also coupled with strain.
(iii) Shear strains are at most only very weakly coupled to antiferromagnetic ordering. No overt evidence of strain coupling has been observed in association with the ferromagnetic ordering at high temperatures but it remains possible that the ferromagnetic signal comes from an impurity phase.
(iv) A relatively high plateau of acoustic loss below ~300 K can be understood in terms of relaxations of strained regions within a tweed microstructure. It is postulated that the mobility of these regions reduces below ~80–100 K due to pinning by defects with a spread of relaxation times.
(v) The combined elastic and anelastic data are permissive of the view that PFN has substantial strain heterogeneity at a mesoscopic length scale, which must inevitably influence the formation of the low temperature spin glass if there is any dependence of the spin configurations on strain. This heterogeneity is superimposed on the slight chemical heterogeneity of the present sample.
(vi) Varying the degree of local chemical ordering is likely to provide a methodology for tuning the strength and dynamics of magnetoelectric coupling but also gives rise to complex ferroelastic properties which must be taken account of.

Acknowledgments

This work was supported in part by a grant from the Engineering and Physical Sciences Research Council (EP/I036079/1) which is gratefully acknowledged. The RUS facilities in Cambridge were established with support from the Natural Environment Research Council (grant numbers NE/B505738/1 and NE/F17081/1). I Buisman is thanked for collecting the electron microprobe data. HS and SED acknowledge support from the Winton Programme for the Physics of Sustainability, and HS acknowledges support from the Funai Foundation for Information Technology. JAS gratefully acknowledges the hospitality of the Max Planck Institute for Chemical Physics of Solids. Funding to support this research (to RJH) was also obtained from the European Union's Seventh Framework Programme (FP/2007-2013)/ ERC grant agreement 3207500. The original data presented in figures can be accessed from https://eprints.esc.cam.ac.uk/3326/.

Appendix: Strain analysis

No single data set for the lattice parameters appears to be available for PFN through a sufficiently wide temperature interval that would allow the full determination of spontaneous strains due to coupling with the magnetic and ferroelectric order parameters. There are sufficient data in the literature to estimate their form and magnitude, however. The reference structure is cubic, $Pm\bar{3}m$, and there are three subgroup structures belonging to irreducible representation Γ_4^- to consider: $P4mm$, $R3m$, Cm. These have order parameter components (0,0,q_3), (q_1,q_2,q_3) with $q_1 = q_2 = q_3$ and (q_1,q_2,q_3) with $q_1 = q_2 \neq q_3$, respectively. (If the $2 \times 2 \times 2$ cation ordered structure with space group $Fm\bar{3}m$ is the parent structure, the equivalent subgroups are $I4mm$, $R3m$, Cm [134] and the same strain/order parameter relationships apply). As shown in figure 2 of Howard and Stokes [134], the sequence $Pm\bar{3}m \rightarrow P4mm \rightarrow Cm$ can occur via two second order transitions, whereas $P4mm \rightarrow R3m$ is necessarily first order. An additional question is whether there are two instabilities, and hence two critical temperatures, or only one. If the low temperature structure is rhombohedral there would most likely only be one instability but if it is monoclinic, there could be two separate instabilities determined, for example, by two different soft optic modes.

A full Landau expansion for the Γ_4^- order parameter is well known and is reproduced here from Carpenter *et al* [135].

$$
\begin{aligned}
G = {} & \frac{1}{2}a\Theta_s\left(\coth\left(\frac{\Theta_s}{T}\right) - \coth\left(\frac{\Theta_s}{T_c}\right)\right)(q_1^2 + q_2^2 + q_3^2) \\
& + \frac{1}{4}b(q_1^2 + q_2^2 + q_3^2)^2 + \frac{1}{4}b'(q_1^4 + q_2^4 + q_3^4) \\
& + \frac{1}{6}c(q_1^2 + q_2^2 + q_3^2)^3 + \frac{1}{6}c'(q_1q_2q_3)^2 \\
& + \frac{1}{6}c''(q_1^2 + q_2^2 + q_3^2)(q_1^4 + q_2^4 + q_3^4) \\
& + \lambda_1 e_a(q_1^2 + q_2^2 + q_3^2) + \lambda_2\left[\sqrt{3}\,e_o(q_1^2 - q_2^2)\right. \\
& \left. + e_t(2q_3^2 - q_1^2 - q_2^2)\right] + \lambda_3(e_4q_3q_2 + e_5q_3q_1 + e_6q_1q_2) \\
& + \frac{1}{4}(C_{11}^o - C_{12}^o)(e_o^2 + e_t^2) \\
& + \frac{1}{6}(C_{11}^o + 2C_{12}^o)e_a^2 + \frac{1}{2}C_{44}^o(e_4^2 + e_5^2 + e_6^2).
\end{aligned}
\tag{A.1}
$$

a, b, c, etc, are normal Landau coefficients, Θ_s is the saturation temperature for the Γ_4^- order parameter, T_c is the critical temperature, e_i are components of the second rank

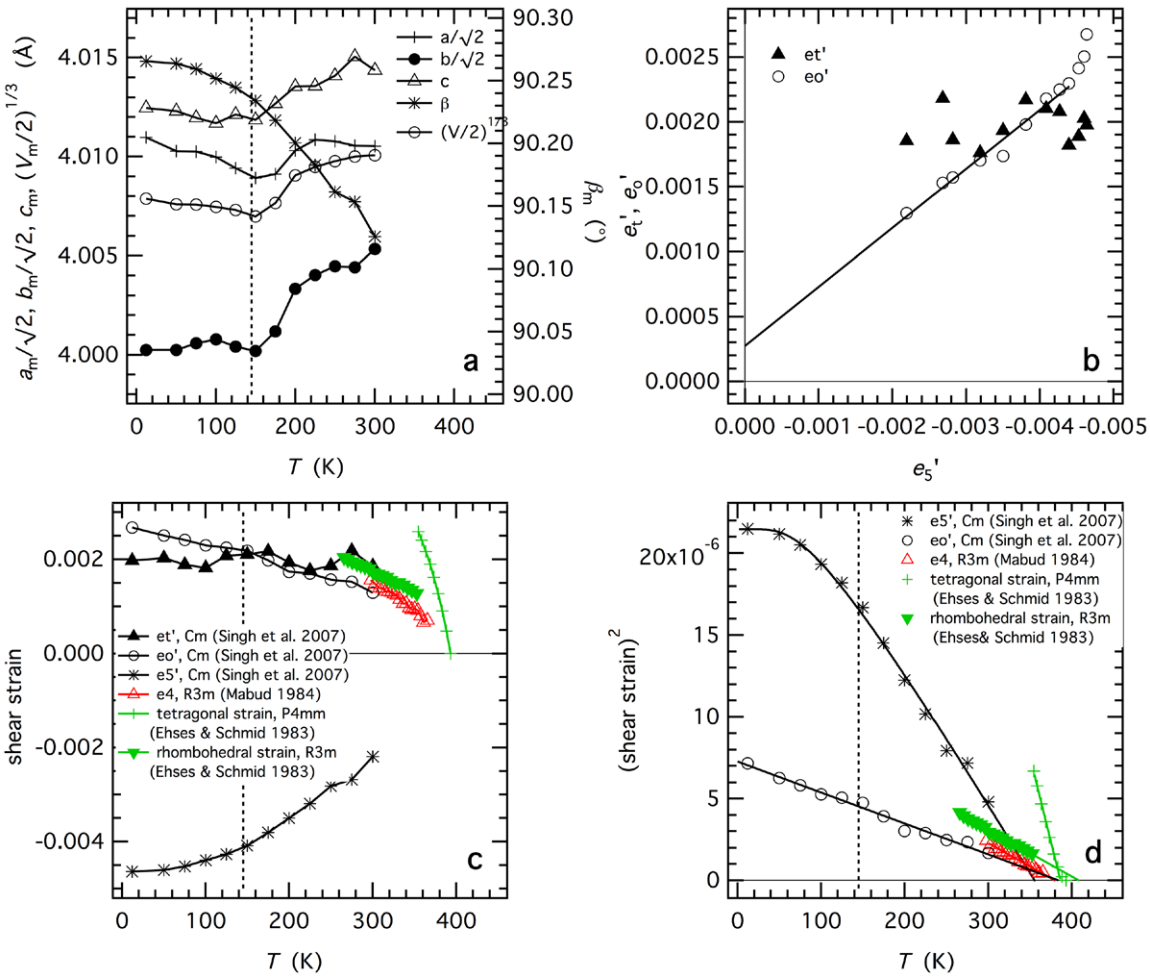

Figure A1. Shear strain variations, defined with respect to a cubic reference structure, calculated from literature data. (a) Lattice parameters of Singh *et al* [18]. The vertical broken line marks the expected Néel point which has been placed at 145 K. (b) Variations of symmetry adapted shear strains calculated from the data in (a). According to equations (A.21)–(A.23), these would be expected to be linearly dependent with a common origin if they derived from coupling with order parameters evolving from a single instability of the form represented by equation (A.1). The straight line through data for e_o' is a guide to the eye. (c) Temperature dependence of shear strains, which would be expected to vary linearly for temperatures approaching the transition point if the transitions were second order in character. (d) Squared values of the tetragonal shear strain have a linear temperature dependence, i.e. $q^4 \propto (T_c - T)$, with $T_c = 386$ K. The other data also have linear dependences, with temperatures for their extrapolation to zero of 384 K (e_o'), 356 K (e_5'), 409 K (rhombohedral shear strain), 380 K (e_4). Note that the function on the right-hand side of equation (A.2) was fit to the data for ${e_5'}^2$, giving $\Theta_s = 120 \pm 14$ K. (Singh *et al* (2007) = [18], Mabud (1984) = [16], Ehses and Schmid (1983) = [7])

strain tensor, with $e_a = (e_1 + e_2 + e_3)$, $e_o = (e_1 - e_2)$ and $e_t = (1/\sqrt{3})(2e_3 - e_1 - e_2)$, λ's are strain/order parameter coupling coefficients and C_{ik}^o are elastic constants of the parent cubic phase. A single instability would give rise to a phase transition at $T = T_c$ if it is second order in character, and the order parameter would be expected to evolve with temperature according to

$$q^2 \propto \left(\coth\left(\frac{\Theta_s}{T_c}\right) - \coth\left(\frac{\Theta_s}{T}\right)\right). \tag{A.2}$$

If the monoclinic structure depends on contributions from two separate instabilities with different critical temperatures, the separate order parameters will be coupled and their evolution below the second transition will be more complicated. The combined effects will be seen in the evolution of the strains which, in principle, should reveal the overall pattern of behaviour.

Setting the equilibrium condition $\partial G/\partial e = 0$ gives strain/order parameter relationships as

$$e_a = (e_1' + e_2' + e_3') = -\frac{\lambda_1(q_1^2 + q_2^2 + q_3^2)}{\frac{1}{3}(C_{11}^o + 2C_{12}^o)} \tag{A.3}$$

$$e_o = -e_6' = -\frac{\sqrt{3}\,\lambda_2(q_1^2 - q_2^2)}{\frac{1}{2}(C_{11}^o - C_{12}^o)} \tag{A.4}$$

$$e_t = \frac{1}{\sqrt{3}}(2e_3' - e_1' - e_2') = -\frac{\lambda_2(2q_3^2 - q_1^2 - q_2^2)}{\frac{1}{2}(C_{11}^o - C_{12}^o)} \tag{A.5}$$

$$e_4 = \frac{1}{\sqrt{2}}(e_5' + e_4') = -\frac{\lambda_3 q_3 q_2}{C_{44}^o} \tag{A.6}$$

$$e_5 = \frac{1}{\sqrt{2}}(e_5' - e_4') = -\frac{\lambda_3 q_3 q_1}{C_{44}^o} \tag{A.7}$$

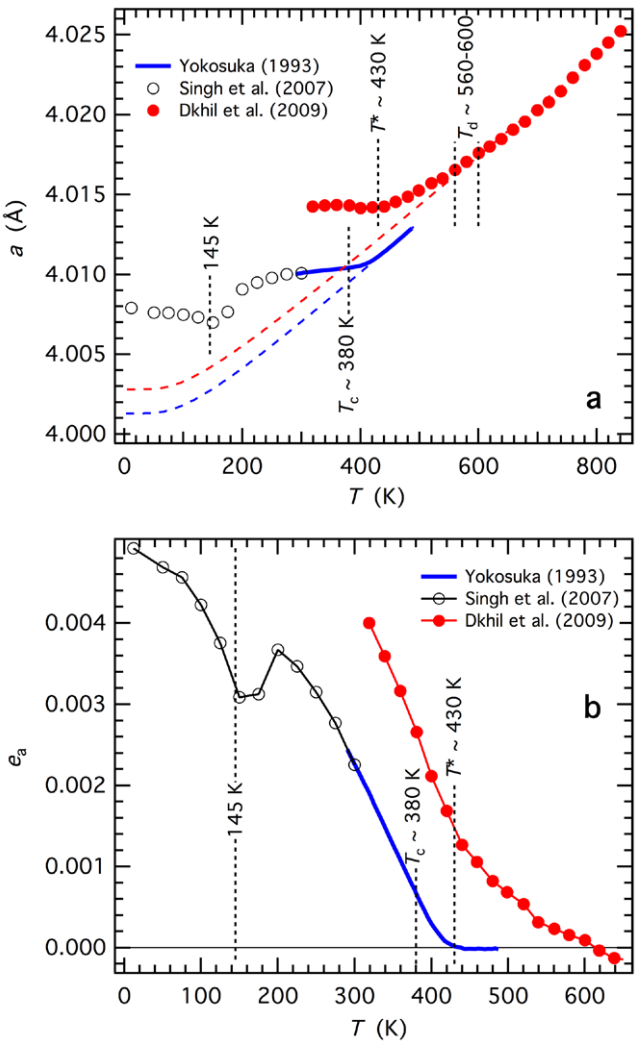

Figure A2. Variations of (a) the cubic and pseudocubic lattice parameters for PFN and (b) the volume strains, e_a, derived from them. Thermal expansion data of Yokosuka [56] were scaled so as to fit with the *Cm* structure at room temperature. Dashed lines in (a) are representations of the reference parameter a_o obtained by fitting of equation (A.24), with $\Theta_{s,ao}$ set at 150 K, to data of Dkhil *et al* [74] in the interval 560–841 K and to data of Yokosuka [56] in the interval 290–360 K. 380 K is the value of T_c reported for the sample of Yokosuka [56], while 430 K and 560–600 K are values of T^* and T_d given by Dul'kin *et al* [12]. For completeness, the value of T_N is shown as 145 K.

$$e_6 = (e_1' - e_2') = -\frac{\lambda_3 q_1 q_2}{C_{44}^o}. \tag{A.8}$$

Here, two alternative reference systems are used for the strains: e_1 to e_6 are for crystallographic axes of the cubic phase parallel to reference axes *X*, *Y* and *Z*, while e_1' to e_6' have [110] // *X*, [$\bar{1}$10] // *Y* and [001] // *Z*.

Values for the strains are obtained from lattice parameters by making use of the equations of Schlenker *et al* [136], and following Redfern and Salje [137], Carpenter *et al* [138]. For the tetragonal structure the non-zero strains are given by

$$e_1 = e_2 = \frac{a - a_o}{a_o} \tag{A.9}$$

$$e_3 = \frac{c - a_o}{a_o}, \tag{A.10}$$

where a_o is the lattice parameter of the cubic reference phase extrapolated into the stability field of the tetragonal structure. In this case

$$e_a \propto e_t \propto q_3^2. \tag{A.11}$$

For the rhombohedral structure the strains are

$$e_1 = e_2 = e_3 \approx \frac{a - a_o}{a_o} \tag{A.12}$$

$$e_4 = e_5 = e_6 = \frac{a}{a_o}\cos\alpha \approx \cos\alpha \tag{A.13}$$

and the relationship with the order parameter is

$$e_a \propto e_t \propto q_3^2. \tag{A.14}$$

For the monoclinic structure the strains are most conveniently defined with respect to the alternative reference axes, giving,

$$e_1' = \frac{a_m - \sqrt{2}\,a_o}{\sqrt{2}\,a_o} \tag{A.15}$$

$$e_2' = \frac{b_m - \sqrt{2}\,a_o}{\sqrt{2}\,a_o} \tag{A.16}$$

$$e_3' = \frac{c_m \sin\beta_m^* - a_o}{a_o} \approx \frac{c_m - a_o}{a_o} \tag{A.17}$$

$$e_4' = e_6' = 0 \tag{A.18}$$

$$e_5' = \frac{c_m}{a_o}\cos\beta_m^* \approx \beta_m, \tag{A.19}$$

where a_m, b_m, c_m and β_m are lattice parameters of the *Cm* structure, and $\beta_m^* = 180 - \beta_m$. The strain/order parameter relationships are

$$e_a = (e_1' + e_2' + e_3') \propto (2q_1^2 + q_3^2) \tag{A.20}$$

$$e_t' = \frac{1}{\sqrt{3}}(2e_3' - e_1' - e_2') \propto (q_3^2 - q_1^2) \tag{A.21}$$

$$e_o' = (e_1' - e_2') \propto q_1^2 \tag{A.22}$$

$$e_5' \propto q_1 q_3. \tag{A.23}$$

Lattice parameter variations and strains calculated from them for the cubic, rhombohedral and monoclinic structures are given in figures A1 and A2. Data for the monoclinic structure (figure A1(a)) are from Singh *et al* [18]. Since these do not extend into the stability field of the cubic structure, it is not possible to determine values of a_o by extrapolation or to determine the volume strain, e_a. However, use of the approximation $a_o = (V_m/2)^{1/3}$, where V_m is the unit cell volume, allows the shear strains to be determined without significant loss of precision. These are plotted against each other in figure A1(b) and as a function of temperature in figure A1(c). If there is only one

instability responsible for changes in the order parameters, e_t', e_o' and e_5' would be expected to be linearly dependent on each other with a common origin. From the variations shown in figure A1(b) this is clearly not the case.

Mabud [16] treated the low symmetry structure of PFN as being rhombohedral and obtained values for the lattice angle, α, from single crystal x-ray diffraction patterns. No evidence was found for a second transition and $T_c \sim 393$ K derived from measurements of the dielectric constant was presumed to be for the symmetry change cubic–rhombohedral. Values of e_4 (~cosα) calculated from these data are shown in figure A1(c). The variation of e_4 with temperature is non-linear but e_4^2 varies linearly with temperature and extrapolates to zero at 380 K (figure A1(d)). If there is only one transition, the implication would be that it is close to tricritical in character, i.e. $q^4 \propto (T_c - T)$, but the discrepancy from T_c given by the dielectric data suggests that a small field of stability for the tetragonal structure has been missed. Tetragonal and rhombohedral shear strains have also been determined from the separation of the splitting of selected powder diffraction lines, as given by Ehses and Schmid [7] who reported the structural sequence cubic → tetragonal → rhombohedral with falling temperature. These are also non-linear functions of temperature (figure A1(c)). Squared values of the tetragonal shear strain have a linear temperature dependence and go to zero at $T_c = 386$ K, consistent with tricritical character for the cubic–tetragonal transition. If there is only one instability driving the two transitions, as in $BaTiO_3$, it would be expected that the square of the rhombohedral shear strain should also be linear and extrapolate to zero at the same value of T_c. The variation is linear, but the extrapolation to zero occurs at 409 K. Squared values of e_o' and e_5' for the monoclinic structure are similarly close to linear, with extrapolations to zero at ~384 and ~356 K, respectively. (Note that the data for e_5' have been fit with the function on the right of equation A2 to include the influence of order parameter saturation).

This analysis of shear strains shows, firstly, that, in keeping with the known ferroelectric behaviour of $PbTiO_3$ [139], the cubic–tetragonal transition is close to tricritical in character. Secondly, a separate transition from monoclinic or rhombohedral to cubic would also be close to tricritical except that it seems to involve the development of a second instability, rather than being described in full by equation (A.1). Finally, none of the shear strains shows any anomaly in the vicinity of T_N (figure A1(c)), implying that the antiferromagnetic order parameter is not coupled to any lattice shear.

Variations of the volume strain for PFN have been estimated by making use of lattice parameters reported in Dkhil *et al* [74] and of (unpoled) thermal expansion data reported by Yokosuka [56]. These are shown in figure A2. Values of the cubic lattice parameter have been derived from the primary data of Yokosuka [56] by scaling them with respect to the room value of $(V_m/2)^{1/3}$ from Singh *et al* [18]. Following Carpenter *et al* [135], values of the reference parameter of the parent cubic phase, a_o, have been obtained by fitting the function [140–144]

$$a_o = a_1 + a_2\Theta_{s,ao}\coth\left(\frac{\Theta_{s,ao}}{T}\right), \qquad (A.24)$$

with $\Theta_{s,ao}$ set at 150 K. The resulting values of the volume strain, $e_a = 3e_1 = 3(a - a_o)/a_o$, are shown in figure A2(b). These are subject to large uncertainties, in comparison with the shear strain variations, because of the uncertainty in placing a_o, but they at least show the form of the volume strain variation.

From figure A2, it is clear that the volume strain is positive and varies continuously through the transition interval of the ferroelectric transition(s). Dielectric data from the sample of Yokosuka [56] gave an independent estimate of T_c as 380 K, but an obvious break in slope in the strain data occurs ~40 K above this which is close to the value of $T^* \sim 430$ K proposed by Dul'kin *et al* [12]. Although slightly arbitrary, the conjoining of data from Singh *et al* [18] with those of Yokosuka [56] shows a small negative volume strain in the vicinity of the expected value of T_N. This amounts only to ~1‰ but the opposite sign implies that coupling between the ferroelectric and antiferromagnetic order parameters would be unfavourable on the basis of a common strain mechanism alone. Values of e_a derived from the data of Dkhil *et al* [74] are substantially greater but also show a break in slope near 430 K. Lattice parameter determination for a thin film on $SrTiO_3$ substrate [49] reveals the same pattern of positive volume strain associated with the ferroelectric transition and negative volume strain associated with the antiferromagnetic ordering transition.

References

[1] Sanchez D A, Ortega N, Kumar A, Roque-Malherbe R, Polanco R, Scott J F and Katiyar R S 2011 *AIP Adv.* **1** 042169

[2] Sanchez D A, Ortega N, Kumar A, Sreenivasulu G, Katiyar R S, Scott J F, Evans D M, Arredondo-Arechavala M, Schilling A and Gregg J M 2013 *J. Appl. Phys.* **113** 074105

[3] Schiemer J *et al* 2014 *Adv. Funct. Mater.* **2014** 1

[4] Glinchuk M D, Eliseev E A and Morozovska A N 2014 *J. Appl. Phys.* **116** 054101

[5] Evans D M, Schilling A, Kumar A, Sanchez D, Ortega N, Arredondo M, Katiyar R S, Gregg J M and Scott J F 2013 *Nat. Commun.* **4** 1534

[6] Bokov V A, Myl'nikova I E and Smolenskii G A 1962 *Sov. Phys.—JETP* **15** 447–50

[7] Ehses K H and Schmid H 1983 *Z. Krist.* **162** 64–6

[8] Bonny V, Bonin M, Sciau P, Schenk K J and Chapuis G 1997 *Solid State Commun.* **102** 347–52

[9] Levstik A, Filipic C and Holc J 2008 *J. Appl. Phys.* **103** 066106

[10] Brunskill I H, Schmid H and Tissot P 1981 *Ferroelectrics* **37** 547–50

[11] Raevski I P, Kubrin S P, Raevskaya S I, Prosandeev S A, Malitskaya M A, Titov V V, Sarychev D A, Blazhevich A V and Zakharchenko I N 2012 *IEEE Trans. Ultrason. Ferroelectr. Freq. Control* **59** 1872–8

[12] Dul'kin E, Kania A and Roth M 2014 *Mater. Res. Express* **1** 016105

[13] Bhat K C, Keer H V and Biswas A B 1974 *J. Phys. D: Appl. Phys.* **7** 2077–80

[14] Platonov G L, Drobyshev L A, Tomashpol'skii Yu Ya and Venevtsev Yu N 1970 *Sov. Phys. Cryst.* **14** 692–5
[15] Brunskill I H, Boutellier R, Depmeier W and Schmid H 1982 *J. Cryst. Growth* **56** 541–6
[16] Mabud S A 1984 *Phase Trans.* **4** 183–200
[17] Lampis N, Sciau P and Geddo Lehmann A 1999 *J. Phys.: Condens. Matter* **11** 3489–500
[18] Singh S P, Pandey D, Yoon S, Baik S and Shin N 2007 *Appl. Phys. Lett.* **90** 242915
[19] Fuentes-Montero L, Montero-Cabrera M E, Calzada L, Pérez De la Rosa M, Raymond O, Font R, García M, Mehta A, Torres M and Fuentes L 2009 *Integr. Ferroelectr.* **101** 101–13
[20] Matteppanavar S, Angadi B and Rayaprol S 2012 *AIP Conf. Proc.* **1512** 1232–3
[21] Matteppanavar S, Angadi B and Rayaprol S 2014 *Physica* B **448** 229–32
[22] Mesquita A, Fraygola B M, Mastelaro V R and Eiras J A 2012 *Appl. Phys. Lett.* **100** 172907
[23] Ivanov S A, Tellgren R, Rundlof H, Thomas N W and Ananta S 2000 *J. Phys.: Condens. Matter* **12** 2393–400
[24] Stock C, Dunsiger S R, Mole R A, Li X and Luo H 2013 *Phys. Rev.* B **88** 094105
[25] Howes B, Pelizzone M, Fischer P, Tabares-Munoz C, Rivera J-P and Schmid H 1984 *Ferroelectrics* **54** 317–20
[26] Chillal S, Thede M, Litterst F J, Gvasaliya S N, Shaplygina T A, Lushnikov S G and Zheludev A 2013 *Phys. Rev.* B **87** 220403
[27] Pietrzak J, Maryanowska A and Leciejewicz J 1981 *Phys. Status Solidi a* **65** K79–82
[28] Astrov D N, Al'shin B I, Zorin R V and Drobyshev L A 1969 *Sov. Phys.—JETP* **28** 1123–5
[29] Watanabe T and Kohn K 1989 *Phase Trans.* **15** 57–68
[30] Raymond O, Font R, Portelles J and Siqueiros J M 2011 *J. Appl. Phys.* **109** 094106
[31] Wang J T, Zhang C, Shen Z X and Feng Y 2004 *Ceram. Int.* **30** 1627–30
[32] Gao X S, Chen X Y, Yin J, Wu J, Liu Z G and Wang M 2000 *J. Mater. Sci.* **35** 5421–5
[33] Yang Y, Liu J-M, Huang H B, Zou W Q, Bao P and Liu Z G 2004 *Phys. Rev.* B **70** 132101
[34] Lente M H, Guerra J D S, de Souza G K S, Fraygola B M, Raigoza C F V, Garcia D and Eiras J A 2008 *Phys. Rev.* B **78** 054109
[35] Font R, Alvarez G, Raymond O, Portelles J and Siqueiros J M 2008 *Appl. Phys. Lett.* **93** 172902
[36] Correa M, Kumar A, Katiyar R S and Rinaldi C 2008 *Appl. Phys. Lett.* **93** 192907
[37] Fraygola B, Frizon N, Lente M H, Coelho A A, Garcia D and Eiras J A 2013 *Acta Mater.* **61** 1518–24
[38] Maryanowska A and Pietrzak J 1994 *Ferroelectrics* **162** 81–5
[39] Blinc R, Cevc P, Zorko A, Holc J, Kosec M, Trontelj Z, Pirnat J, Dalal N, Ramachandran V and Krzystek J 2007 *J. Appl. Phys.* **101** 033901
[40] Kumar A, Katiyar R S, Rinaldi C, Lushnikov S G and Shaplygina T A 2008 *Appl. Phys. Lett.* **93** 232902
[41] Laguta V V, Glinchuk M D, Marysko M, Kuzian R O, Prosandeev S A, Raevskaya S I, Smotrakov V G, Eremkin V V and Raevski I P 2013 *Phys. Rev.* B **87** 064403
[42] Falqui A, Lampis N, Geddo-Lehmann A and Pinna G 2005 *J. Phys. Chem.* B **109** 22967
[43] Rotaru G M, Roessli B, Amato A, Gvasaliya S N, Mudry C, Lushnikov S G and Shaplygina T A 2009 *Phys. Rev.* B **79** 184430
[44] Kleemann W, Shvartsman V V, Borisov P and Kania A 2010 *Phys. Rev. Lett.* **105** 257202
[45] Majumder S B, Bhattacharya S, Katiyar R S, Manivannan A, Dutta P and Seehra M S 2006 *J. Appl. Phys.* **99** 024108
[46] Fraygola B, Nascimento W J, Coelho A C, Garcia D, Eiras J E 2013 *Phys. Status Solidi a* **210** 1856–60
[47] Yan L, Li J, Suchicital C and Viehland D 2006 *Appl. Phys. Lett.* **89** 132913
[48] Yan L, Zhao X, Li J and Viehland D 2009 *Appl. Phys. Lett.* **94** 192903
[49] Peng W, Lemée N, Karkut M, Dkhil B, Shvartsman V V, Borisov P, Kleemann W, Holc J, Kosec M and Blinc R 2009 *Appl. Phys. Lett.* **94** 012509
[50] Mishra R K, Choudhary R N P and Banerjee A 2010 *J. Phys.: Condens. Matter* **22** 025901
[51] Liu J-M, Li Q C, Gao X S, Yang Y, Zhou X H, Chen X Y and Liu Z G 2002 *Phys. Rev.* B **66** 054416
[52] Yang Y, Huang H B, Liu J-M and Liu Z G 2002 *Ferroelectrics* **280** 75–82
[53] Alvarez G, Font R, Portelles J, Valenzuela R and Zamorano R 2006 *Physica* B **384** 322–5
[54] Yang Y, Huang H-B, Shen H-L, Liu J-M and Liu Z-G 2006 *Trans. Nonferrous Met. Soc. China* **16** 117–21
[55] Yasuda N and Ueda Y 1989 *J. Phys.: Condens. Matter* **1** 497–500
[56] Yokosuka M 1993 *Japan. J. Appl. Phys.* **32** 1142–6
[57] Raymond O, Font R, Suárez-Almodovar N, Portelles J and Siqueiros J M 2005 *J. Appl. Phys.* **97** 084107
[58] Eiras J A, Fraygola B M, Lente M H, Frizon N and Garcia D 2009 *Ferroelectrics* **380** 69–72
[59] Bochenek D, Surowiak Z, Krok-Kowalski J, Poltierova-Vejpravova J 2010 *J. Electroceram.* **25** 122–9
[60] Singh S P, Yusuf S M, Yoon S, Baik S, Shin N and Pandey D 2010 *Acta Mater.* **58** 5381–92
[61] Raevski I P, Kubrin S P, Raevskaya S I, Titov V V, Prosandeev S A, Sarychev D A, Malitskaya M A, Stashenko V V and Zakharchenko I N 2010 *Ferroelectrics* **398** 16–25
[62] Bochenek D and Guzdek P 2011 *J. Magn. Magn. Mater.* **323** 369–74
[63] Fraygola B, Frizon N, Lente M H, Coelho A A, Garcia D and Eiras J A 2011 *Integr. Ferroelectr.* **124** 53–60
[64] Gridnev S A and Kamynin A A 2012 *Phys. Solid State* **54** 1018–20
[65] Bokov A A and Emelyanov S M 1991 *Phys. Status Solidi b* **164** K109–12
[66] Fundora A, Vázquez A, Portelles J, Calderón F and Siqueiros J M 1998 *J. Non-Cryst. Solids* **235–237** 567–9
[67] Bharti C, Choudhary S N and Sinha T P 2008 *J. Surf. Sci. Technol.* **24** 1–10
[68] Darlington C N W 1991 *J. Phys.: Condens. Matter* **3** 4173–85
[69] Raevski I P, Kubrin S P, Raevskaya S I, Sarychev D A, Prosandeev S A and Malitskaya M A 2012 *Phys. Rev.* B **85** 224412
[70] Raevskii I P, Sarychev D A, Bryugeman S A, Reznichenko L A, Shilkina L A, Razumovskaya O N, Nikolaev V S, Vyshatko N P and Salak A N 2002 *Cryst. Rep.* **47** 1012–5
[71] Laguta V V, Rosa J, Jastrabik L, Blinc R, Cevc P, Zalar B, Remskar M, Raevskaya S I and Raevski I P 2010 *Mater. Res. Bull.* **45** 1720–7
[72] García-Flores A F, Tenne D A, Choi Y J, Ren W J, Xi X X and Cheong S W 2011 *J. Phys.: Condens. Matter* **23** 015401
[73] Correa M, Kumar A, Priya S, Katiyar R S and Scott J F 2011 *Phys. Rev.* B **83** 014302
[74] Dkhil B, Gemeiner P, Al-Barakaty A, Bellaiche L, Dul'kin E, Mojaev E and Roth M 2009 *Phys. Rev.* B **80** 064103
[75] Ananta S and Thomas N W 1999 *J. Eur. Ceram. Soc.* **19** 1873–81
[76] Rayevsky I P, Bokov A A, Bogatin A S, Emelyanov S M, Malitskaya M A and Prokopalo O I 1992 *Ferroelectrics* **126** 191–6
[77] Kuzian R O, Kondakova I V, Daré A M and Laguta V V 2014 *Phys. Rev.* B **89** 024402
[78] Kuzian R O, Laguta V V and Richter J 2014 *Phys. Rev.* B **90** 134415

[79] Meng X, Baba-Kishi K Z, Chan H L, Choy C L and Luo H S 2004 *Ferroelectrics* **303** 69–73
[80] Fraygola B, Mesquita A, Coelho A A, Garcia D, Mastelaro V R and Eiras J A 2013 *Phys. Status Solidi a* **210** 386
[81] Zachariasz R and Bochenek D 2008 *Eur. Phys. J. Spec. Top.* **154** 253–6
[82] Bochenek D and Zachariasz R 2009 *Arch. Met. Mater.* **54** 903–10
[83] Rietveld H M 1969 *J. Appl. Cryst.* **2** 65–71
[84] Rodriguez-Carvajal J, Fernandez-Diaz M T and Martinez J L 1991 *J. Phys.: Condens. Matter* **3** 3215–34
[85] Roberts A P, Pike C R and Verosub K L 2000 *J. Geophys. Res.* **105** 28461–75
[86] Pike C R, Roberts A P and Verosub K L 1999 *J. Appl. Phys.* **85** 6660–7
[87] Pike C R, Roberts A P and Verosub K L 2001 *Geophys. J. Int.* **145** 721–30
[88] Pike C R, Roberts A P, Dekkers M J and Verosub K L 2001 *Phys. Earth Planet. Int.* **126** 11–25
[89] Mayergoyz I D 1986 *IEEE Trans. Magn.* **22** 603–8
[90] Harrison R J and Feinberg J M 2008 *Geochem. Geophys. Geosyst.* **9** Q05016
[91] Egli R 2013 *Glob. Planet. Change* **110** 302–20
[92] McKnight R E A, Carpenter M A, Darling T W, Buckley A and Taylor P A 2007 *Am. Mineral.* **92** 1665–72
[93] McKnight R E A, Moxon T, Buckley A, Taylor P A, Darling T W and Carpenter M A 2008 *J. Phys.: Condens. Matter* **20** 075229
[94] Zhang Z, Koppensteiner J, Schranz W, Betts J B, Migliori A and Carpenter M A 2010 *Phys. Rev.* B **82** 014113
[95] Carpenter M A, Bryson J F J, Catalan G, Zhang S J and Donnelly N J 2012 *J. Phys.: Condens. Matter* **24** 045902
[96] Kania A, Talik E and Kruczek M 2009 *Ferrolectrics* **391** 114–21
[97] Havlicek R, Vejpravova J P and Bochenek D 2009 *J. Phys.: Conf. Ser.* **200** 012058
[98] Heslop D and Roberts A P 2012 *Geochem. Geophys. Geosyst.* **13** Q12Z40
[99] McKnight R E A, Howard C J and Carpenter M A 2009 *J. Phys.: Condens. Matter* **21** 015901
[100] Carpenter M A, Howard C J, McKnight R E A, Migliori A, Betts J B and Fanelli V R 2010 *Phys. Rev.* B **82** 134123
[101] Aktas O, Salje E K H, Crossley S, Lampronti G I, Whatmore R W, Mathur N D and Carpenter M A 2013 *Phys. Rev.* B **88** 174112
[102] Nataf G F, Li Q, Liu Y, Withers R L, Driver S L and Carpenter M A 2013 *J. Appl. Phys.* **113** 124102
[103] Aktas O, Carpenter M A and Salje E K H 2013 *Appl. Phys. Lett.* **103** 142902
[104] Ozdemir O, Dunlop D J and Berquo T S 2008 *Geochem. Geophys. Geosyst.* **9** Q10Z01
[105] Popovici M *et al* 2004 *Chem. Mater.* **16** 5542–8
[106] Jin J, Ohkoshi S and Hashimoto K 2004 *Adv. Mater.* **16** 48–51
[107] Gich M, Roig A, Frontera C, Molins E, Sort J, Popovici M, Chouteau G, Martin D, Marero Y and Nogués J 2005 *J. Appl. Phys.* **98** 044307
[108] Gich M, Frontera C, Roig A, Fontcuberta J, Molins E, Bellido N, Simon Ch and Fleta C 2006 *Nanotechnology* **17** 687–91
[109] Gich M *et al* 2006 *Chem. Mater.* **18** 3889–97
[110] Gil D M, Nieva G, Franco D G, Gómez M I and Carbonio R E 2013 *Mater. Chem. Phys.* **141** 355–61
[111] Gorev M V, Flerov I N, Sciau Ph, Bondarev V S and Geddo Lehmann A 2004 *Ferroelectrics* **307** 127–36
[112] Rehwald W 1973 *Adv. Phys.* **22** 712–55
[113] Lüthi B and Rehwald W 1981 *Top. Curr. Phys.* **23** 131–84
[114] Carpenter M A and Salje E K H 1998 *Eur. J. Mineral.* **10** 693–812
[115] Scott J F 2013 *Europhys. Lett.* **103** 37001–5
[116] Driver S L, Herrero-Albillos J, Bonilla C M, Bartolomé F, Garcia L M, Howard C J and Carpenter M A 2014 *J. Phys.: Condens. Matter* **26** 056001
[117] Wenyuan S, Huimin S, Yening W and Baosheng L 1985 *J. Physique Coll.* **46** C10-609–12
[118] Yening W, Wenyuan S, Xiaohua C, Huimin S and Baosheng L 1987 *Phys. Status Solidi a* **102** 279–85
[119] Salje E K H 1993 *Phase Transitions in Ferroelastic and Coelastic Crystals* (Cambridge: Cambridge University Press)
[120] Chrosch J and Salje E K H 1999 *J. Appl. Phys.* **85** 722–7
[121] Lee W T, Salje E K H and Bismayer U 2005 *Phys. Rev.* B **72** 104116
[122] Lee W T, Salje E K H, Goncalves-Ferreira L, Daraktchiev M and Bismayer U 2006 *Phys. Rev.* B **73** 214110
[123] Carpenter M A and Zhang Z 2011 *Geophys. J. Int.* **186** 279–95
[124] Salje E K H, Ding X, Zhao Z, Lookman T and Saxena A 2011 *Phys. Rev.* B **83** 104109
[125] Carpenter M A, Salje E K H and Howard C J 2012 *Phys. Rev.* B **85** 224430
[126] Harrison R J, Redfern S A T and Salje E K H 2004 *Phys. Rev.* B **69** 144101
[127] Carpenter M A, Buckley A, Taylor P A and Darling T W 2010 *J. Phys.: Condens. Matter* **22** 035405
[128] Viehland D W and Salje E K H 2014 *Adv. Phys.* **63** 267–326
[129] Lee S-B, Lee K-H and Kim H 2002 *Japan. J. Appl. Phys.* **41** 5266–71
[130] Bochenek D 2008 *Eur. Phys. J. Spec. Top.* **154** 15–8
[131] Bochenek D and Dudek J 2008 *Eur. Phys. J. Spec. Top.* **154** 19–22
[132] Raymond O, Font R, Portelles J, Suárez-Almodovar N and Siqueiros J M 2006 *J. Appl. Phys.* **99** 124101
[133] Yang Y, Zhang S T, Huang H B, Chen Y F, Liu Z G and Liu J-M 2005 *Mater. Lett.* **59** 1767–70
[134] Howard C J and Stokes H T 2005 *Acta Crystallogr.* A **61** 93–111
[135] Carpenter M A, Bryson J F J, Catalan G and Howard C J 2012 *J. Phys.: Condens. Matter* **24** 045901
[136] Schlenker J L, Gibbs G V and Boisen M B Jr 1978 *Acta Crystallogr.* A **34** 52–4
[137] Redfern S A T and Salje E 1987 *Phys. Chem. Miner.* **14** 189–95
[138] Carpenter M A, Salje E K H and Graeme-Barber A 1998 *Eur. J. Mineral.* **10** 621–91
[139] Whatmore R W, Clarke R and Glazer A M 1978 *J. Phys. C: Solid State Phys.* **11** 3089–102
[140] Salje E K H, Wruck B and Thomas H 1991 *Z. Phys.* B **82** 399–404
[141] Meyer H-W, Carpenter M A, Graeme-Barber A, Sondergeld P and Schranz W 2000 *Eur. J. Mineral.* **12** 1139–50
[142] Meyer H-W, Marion S, Sondergeld P, Carpenter M A, Knight K S, Redfern S A T and Dove M T 2001 *Am. Mineral.* **86** 566–77
[143] Sondergeld P, Shranz W, Kityk A V, Carpenter M A and Libowitzky E 2000 *Phase Trans.* **71** 189–203
[144] Carpenter M A, Meyer H-W, Sondergeld P, Marion S and Knight K S 2003 *Am. Mineral.* **88** 534–46